Gamma-ray emission from non-blazar AGNs

N. Sahakyan in collaboration with D. Zargaryan, V. Baghmanyan and S. Gasparyan

ICRANet-Armenia

Outline

- Introduction
- Radio Galaxies
- Data analysis
- Spectral and Temporal analysis
- Individual Sources

  Cen A, Fornax A, 3C 120….
- Conclusions

Active Galactic Nuclei

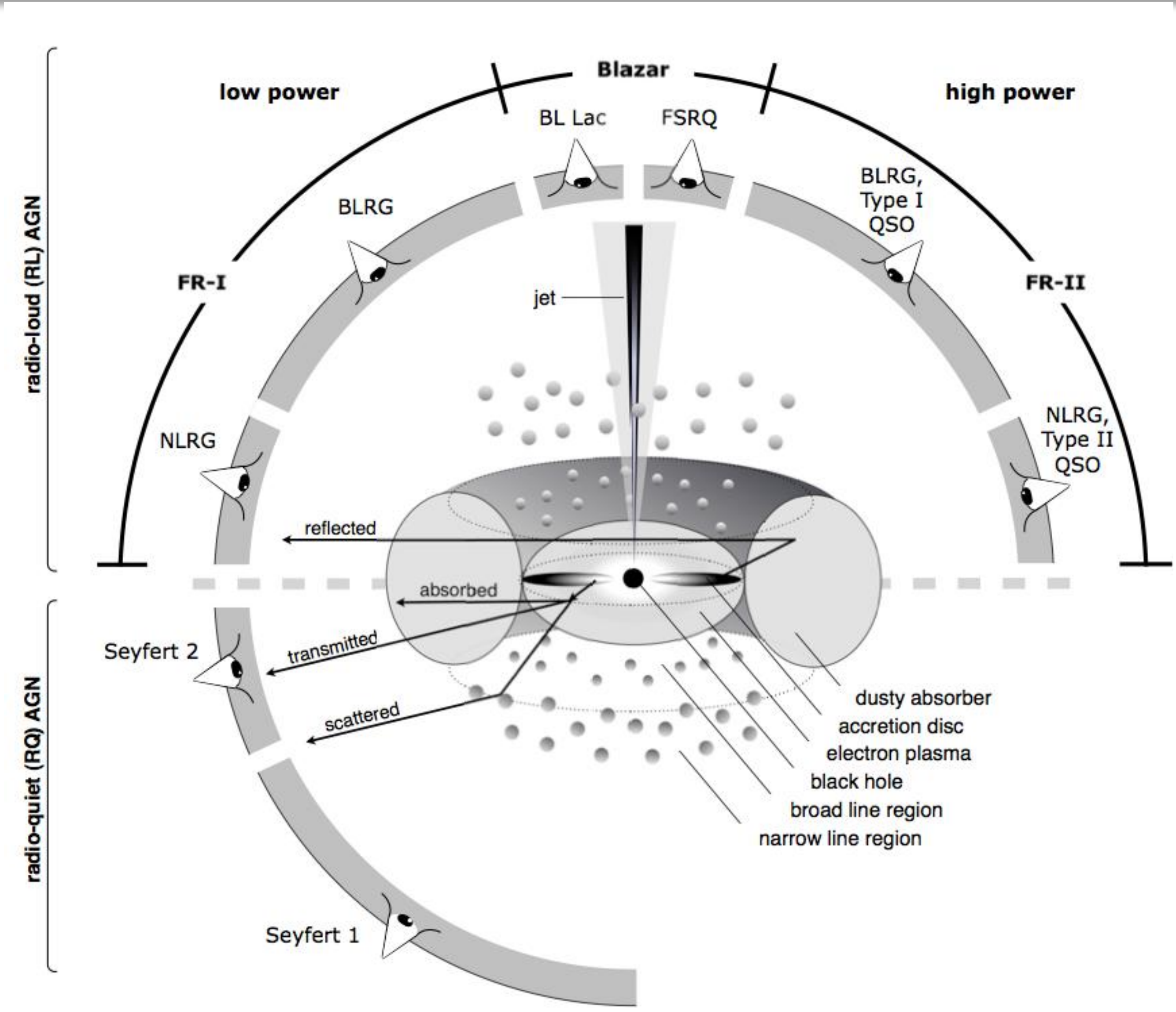

AGN-Unification

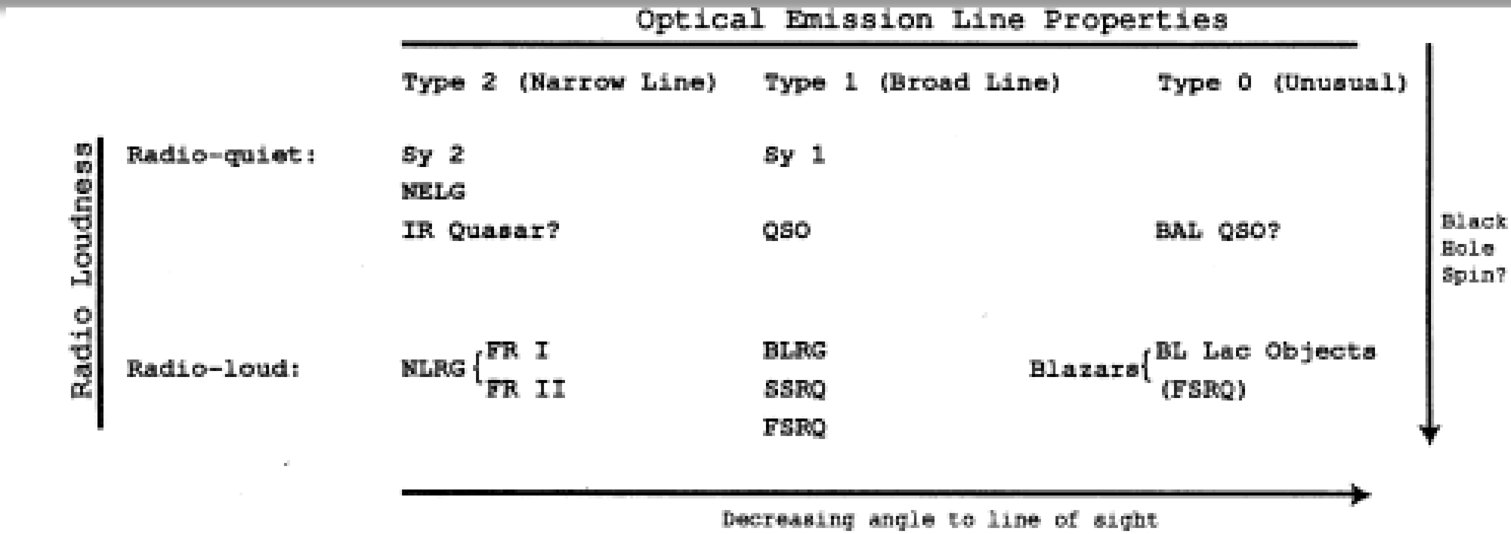

Blazar

- The emission is strongly boosted
- The emission is produced from the compact region in the jet
- Unique possibility to investigate the sub-parsec scale structure of jet

Radio galaxies

✓ The emission from extended regions comparable with jet emission

✓A chance to investigate both the jet and the extended regions

✓ Investigate the particle acceleration and emission over large scales

Radiogalaxies

- Morphology:
  - Core: flat spectrum, unresolved
  - Jets: up to several 100's kpc, steeper spectrum, may contain "knots"
  - Lobes: big amorphous structure, contain "old" particles
  - Hot spots: present in more powerful sources, bright and compact, site of reacceleration

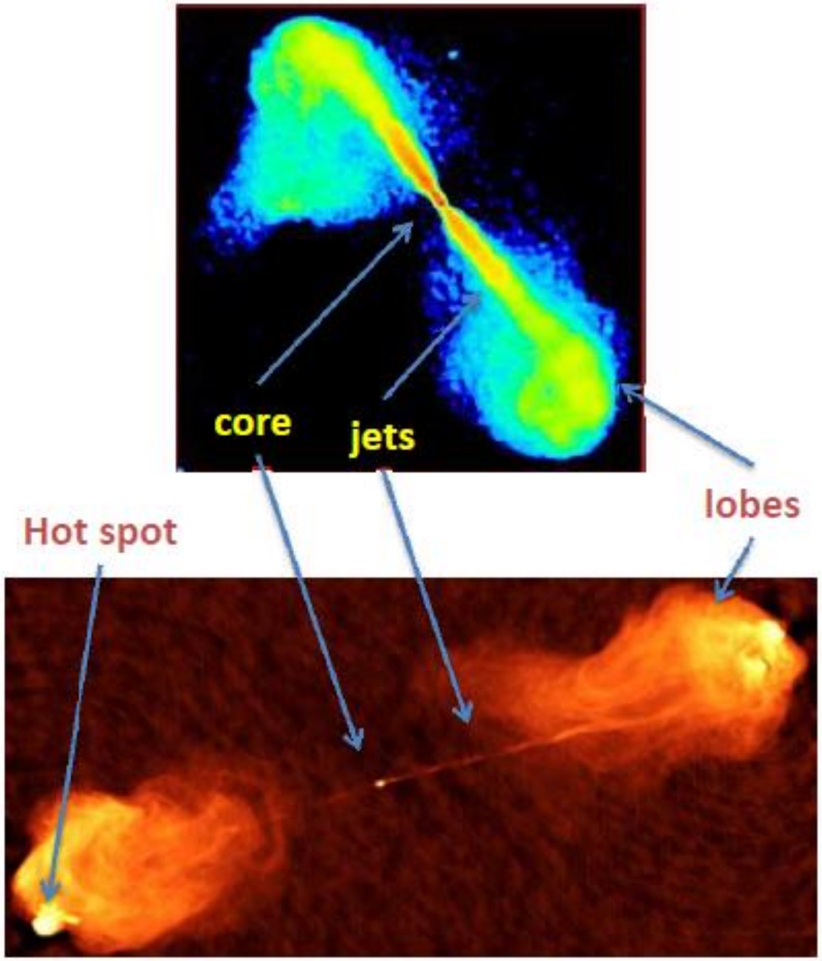

Radiogalaxy types

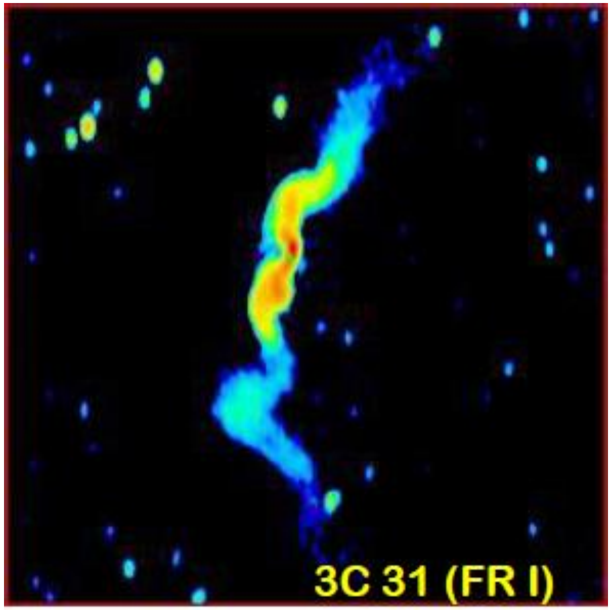

FR I- BL Lac

FR II- FSRQ

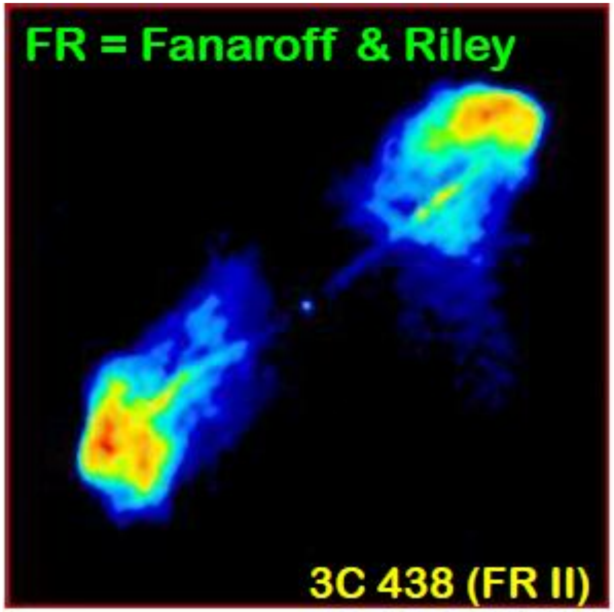

FR I		FR II
$< 10^{41}\, erg\, s^{-1}$	Radio luminosity	$> 10^{41}\, erg\, s^{-1}$
Low Γ	Bulk motion	High Γ
Toward core	Brightness	Toward edges
inefficient energy transport	jet	Collimated, efficient energy transport

Components

M87 jet

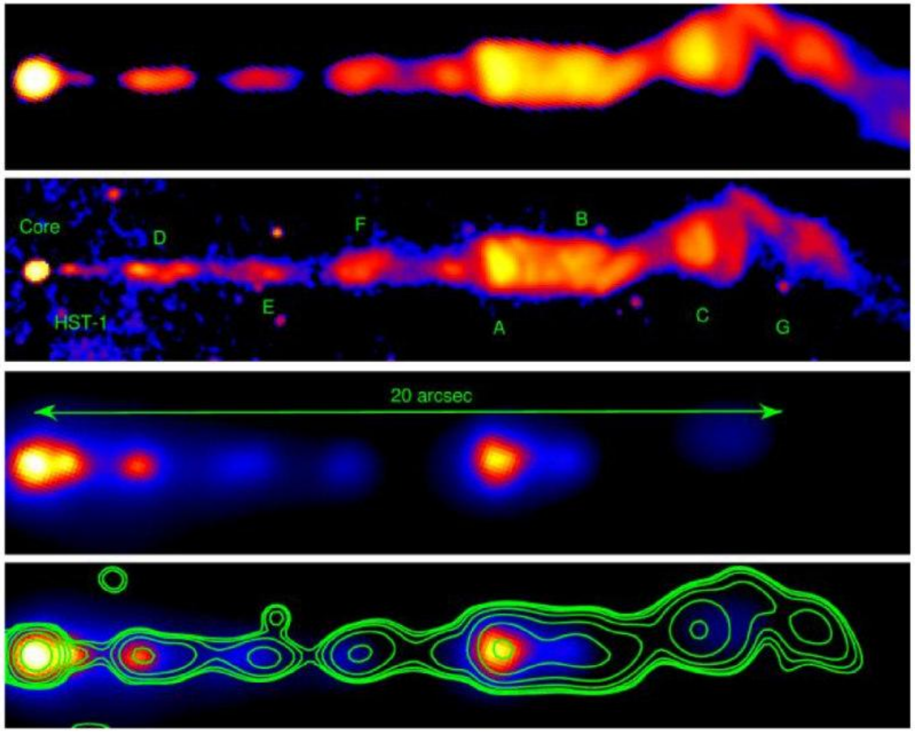

knots

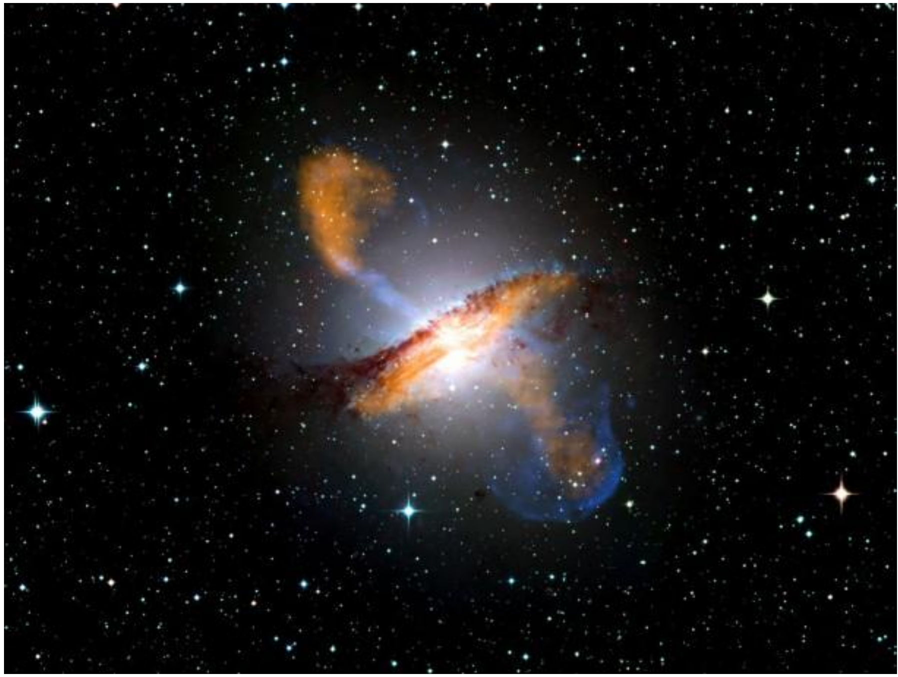

lobes

Observations in the gamma-ray band can help to understand the particle acceleration and emission processes in the components of radio galaxies

Fermi LAT- new view

Large Area Telescope (LAT)

KEY FEATURES

- **20 MeV ➔ >300 GeV photon energies**
- **2.4 Steradian field of view**
- **Operated in scanning mode, so views the entire sky every 3 hours.**
- **Point Source Sensitivity**

$$<6\times10^{-9}\ cm^{-2}s^{-1}$$

Gamma-ray Burst Monitor (GBM)
8 keV - 40 MeV

Third Catalog of AGN

AGN Type	Entire 3LAC	3LAC Clean Sample[a]
All[b]	**1591**	**1444**
FSRQ	**467**	**414**
…LSP	412	366
…ISP	47	42
…HSP	3	2
…no SED classification	5	4
BL Lac	**632**	**604**
…LSP	162	150
…ISP	178	173
…HSP	272	265
…no SED classification	20	16

AGN Type		Entire 3LAC	3LAC Clean Sample[a]
Blazar of Unknown type	**460**	**402**	**125**
…BCU I	57	49	11
…LSP BCU I	26	24	8
…ISP BCU I	11	9	1
…HSP BCU I	13	13	2
…BCU I w/o SED classification	7	3	0
…BCU II	346	308	85
…LSP BCU II	156	129	39
…ISP BCU II	78	70	13
…HSP BCU II	107	105	31
…BCU II w/o SED classification	5	4	2
…BCU III	57	45	29
…LSP BCU III	16	11	9
…ISP BCU III	0	0	0
…HSP BCU III	0	0	0
…BCU III w/o SED classification	41	34	20
Non-blazar AGN	**32**	**24**	**3**
…CSS	2	1	0
…NLSy1	5	5	0
…RG	14	13	2
…SSRQ	5	3	0
…Other AGN	6	2	1

Non-Blazar AGNs

Name	3FGL	2FGL	1FGL	Type
NGC 1218	J0308.6+0408[a]	···	J0308.3+0403[a]	FRI
IC 310	J0316.6+4119[a]	J0316.6+4119	···	FRI/BLL
NGC 1275	J0319.8+4130[a]	J0319.8+4130[a]	J0319.7+4130[a]	FRI
1 H 0323+342	J0325.2+3410[a]	J0324.8+3408[a]	J0325.0+3403[a]	NLSy1
4C+39.12	J0334.2+3915[a]	···	···	FRI/BLL?
TXS 0348+013	J0351.1+0128[a]	···	···	SSRQ
3C 111	J0418.5+3813	···	J0419.0+3811	FRII
Pictor A	J0519.2–4542[a]	···	···	FRII
PKS 0625–35	J0627.0–3529[a]	J0627.1–3528[a]	J0627.3–3530[a]	FRI/BLL
4C+52.17	J0733.5+5153	···	···	AGN
NGC 2484	J0758.7+3747[a]	···	···	FRI
4C+39.23B	J0824.9+3916	···	···	CSS
3C 207	J0840.8+1315[a]	J0840.7+1310	J0840.8+1310	SSRQ
SBS 0846+513	J0849.9+5108[a]	···	···	NLSy1
3C 221	J0934.1+3933	···	···	SSRQ
PMN J0948+0022	J0948.8+0021[a]	J0948.8+0020[a]	J0949.0+0021[a]	NLSy1
PMN J1118–0413	J1118.2–0411[a]	···	···	AGN
B2 1126+37	J1129.0+3705	···	···	AGN
3C 264	J1145.1+1935[a]	···	···	FRI
PKS 1203+04	J1205.4+0412	···	···	SSRQ
M 87	J1230.9+1224[a]	J1230.8+1224[a]	J1230.8+1223[a]	FRI
3C 275.1	J1244.1+1615	···	···	SSRQ
GB 1310+487	J1312.7+4828[a]	J1312.8+4828[a]	J1312.4+4827[a]	AGN
Cen A Core	J1325.4–4301[a]	J1325.6–4300	J1325.6–4300	FRI
Cen A Lobes	J1324.0–4330e	J1324.0–4330e	J1322.0–4515	FRI
3C 286	J1330.5+3023[a]	···	···	SSRQ/CSS
Cen B	J1346.6–6027	J1346.6–6027	···	FRI
Circinus	J1413.2–6518	···	···	Seyfert
3C 303	J1442.6+5156[a]	···	···	FRII
PKS 1502+036	J1505.1+0326[a]	J1505.1+0324[a]	J1505.0+0328[a]	NLSy1
TXS 1613–251	J1617.3–2519	J1617.6–2526c	···	AGN
PKS 1617–235	J1621.1–2331[a]	J1620.5–2320c	···	AGN
NGC 6251	J1630.6+8232[a]	J1629.4+8236	J1635.4+8228[a]	FRI
3C 380	J1829.6+4844[a]	J1829.7+4846[a]	J1829.8+4845[a]	SSRQ/CSS
PKS 2004–447	J2007.8–4429[a]	J2007.9–4430[a]	J2007.9–4430[a]	NLSy1

New Possibilities

PASS 8

Pass 8 provides a full reprocessing of the entire mission dataset, including an improved event reconstruction, a wider energy range, better energy measurements, and significantly increased effective area.

The accumulation of a larger data set allows detailed temporal analysis in short and long time scales, as well as to study the spectrum with better statistics at energies above several GeV.

Analysis

Time period: 2008-2015 (7 years)

Allows to study the variability in short and long time scales which allows to investigate the physical processes, such as particle acceleration and emission mechanisms, origin of flares and size, structure and location of the emission

Energy range: 100 MeV- 300 GeV

The improved statistics allows to investigate the spectrum above GeV energies and test the power-law with exponential cut and broken power-law models. Any cut-off or break in the spectrum will be defined by the cooling of relativistic particles.

Results

Name	Class	Γ	Flux ($\times 10^{9}$ photon $cm^{-2}s^{-1}$)	TS
GB 1310+487	AGN	2.134 ± 0.0207	44.9 ± 1.66	4356
4C+39.23B	CSS	2.456 ± 0.05771	21.2 ± 2.25	410.8
3C 264	FRI	1.998 ± 0.137	2.94 ± 1.14	79.85
NGC 1275	FRI	2.08 ± 0.0055	334 ± 2.29	68871
3C 120	FRI	2.694±0.0593	41.2 ± 5.64	334.89
Cen A Core	FRI	2.672 ± 0.00134	1.93 ± 0.392	6009.16
NGC 2484	FRI	2.11 ± 0.011	2.12 ± 0.056	28.29
Cen B	FRI	2.466±0.05417	77 ± 9.15	341.79
M87	FRI	2.037± 0.0409	19.3±1.85	1061
NGC 6251	FRI	2.356 ± 0.03222	28.8 ± 1.5	979.9
ngc 1218	FRI	2.03±0.08283	7.19±1.58	121.72
IC 310	FRI/BLL	2.036±0.1796	4.43 ±2.78	47.97
TXS 0331+3915	FRI/BLL	1.861 ± 0.1729	1.71 ± 0.962	42.83
PKS 0625-35	FRI/BLL	1.865± 0.04144	11.5 ± 1.19	926.54
3C 111	FRII	2.688±0.0054	46.4 ± 0.32	254.75
3c 303	FRII	2.036±0.19	1.59 ± 0.841	26.77
Pictor A	FRII	2.525±0.1228	13.7 ± 3.75	118.66
SBS 0846+513	NLSy1	2.244±0.02316	46.5 ± 1.85	3134.38
1H0323+342	NLSy1	2.83 ± 0.0267	90.3 ± 2.6	1579.01
PMN J0948+0022	NLSy1	2.618 ± 0.01366	156 ± 2.4	6224.27
PKS 1502+036	NLSy1	2.628 ± 0.03549	52.2 ± 2.39	924.22
PKS 2004-447	NLSy1	2.623 ± 0.0532	28.9 ± 2.35	350.33
3C 207	SSRQ/CSS	2.629 ± 0.0898	16.1 ± 2.39	123.17
3C 221	SSRQ/CSS	2.444 ± 0.09177	9.94 ± 1.78	122.39
3C 275.1	SSRQ/CSS	2.435±0.1186	10.3 ±2.37	96.93
3c 286	SSRQ/CSS	2.7±0.1417	10.5 ± 2.5	60.84
3c 380	SSRQ/CSS	2.422 ± 0.03119	42.7±2.18	1316
PKS 1203+04	SSRQ/CSS	2.684 ± 0.1699	8.56 ± 2.51	31.08

Spectra

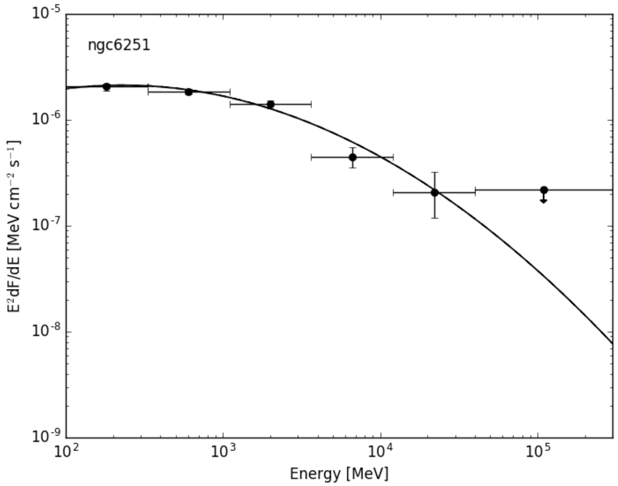
ngc6251
E²dF/dE [MeV cm⁻² s⁻¹]
Energy [MeV]

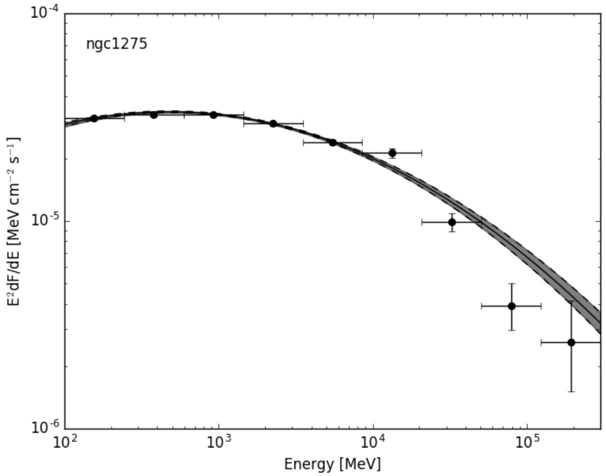
ngc1275
E²dF/dE [MeV cm⁻² s⁻¹]
Energy [MeV]

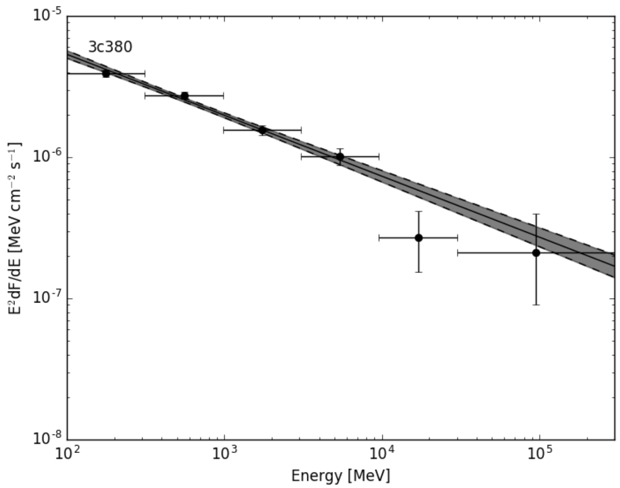
3c380
E²dF/dE [MeV cm⁻² s⁻¹]
Energy [MeV]

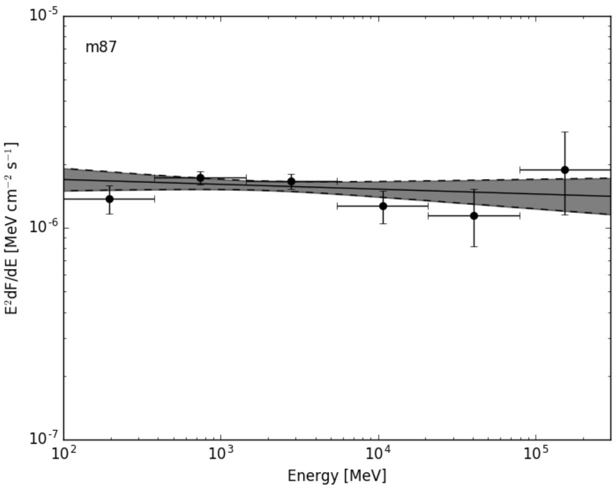
m87
E²dF/dE [MeV cm⁻² s⁻¹]
Energy [MeV]

Sources with hard spectrum

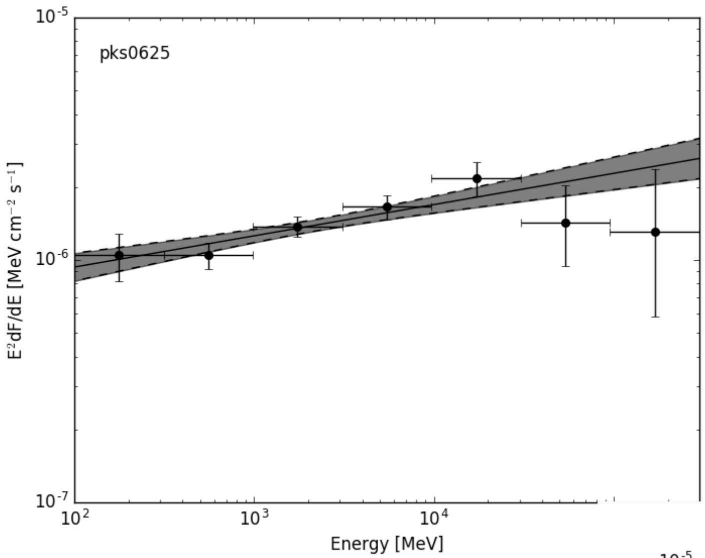

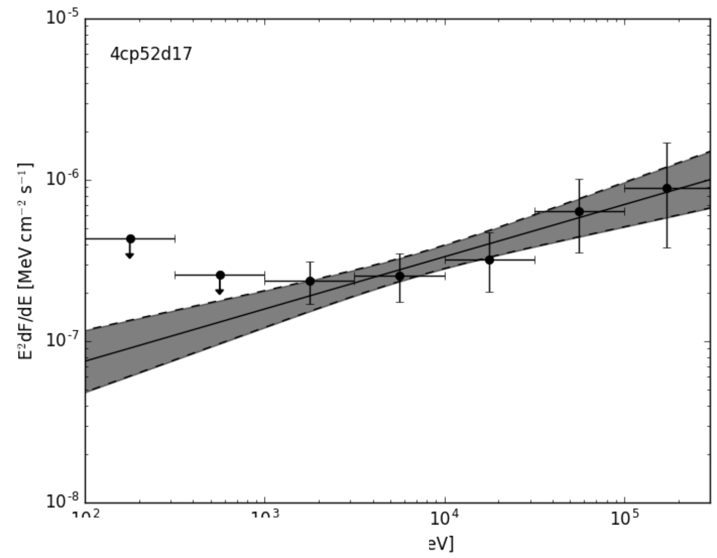

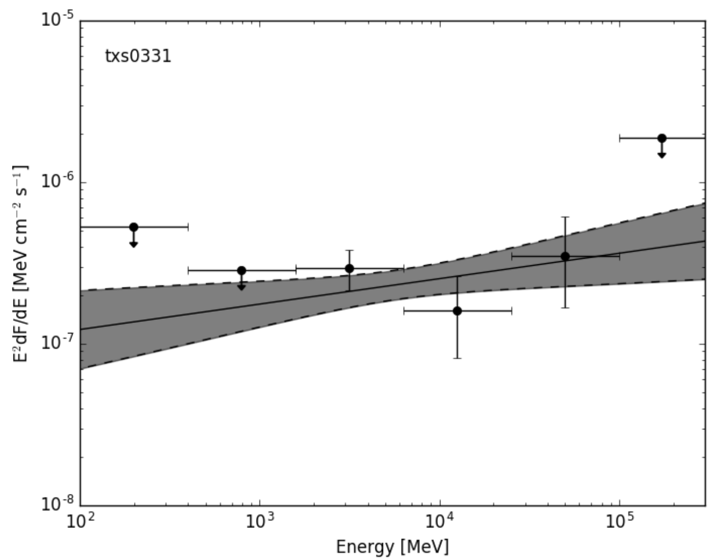

NGC 6251

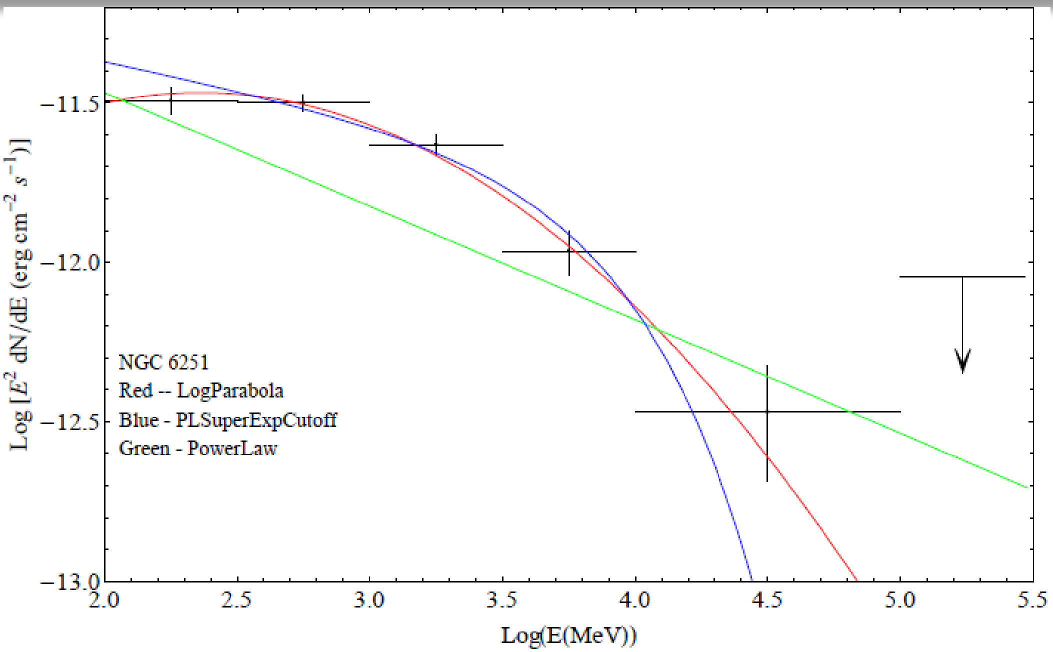

Power-Law

$$\frac{dN}{dE} = (2.69 \pm 0.11) \times 10^{-12} \left(\frac{E}{777.1} \right)^{-2.36 \pm 0.03} cm^{-2} s^{-1} MeV^{-1}$$

The spectrum shows deviation from simple power-law modeling

Power-Law with Exp. cutoff

$$\frac{dN}{dE} = (9.7 \pm 0.99) \times 10^{-13} \left(\frac{E}{1334} \right)^{-2.17 \pm 0.06} Exp\left(-\frac{E}{9834} \right) cm^{-2} s^{-1} MeV^{-1}$$

Log Parabola

$$\frac{dN}{dE} = (2.67 \pm 0.16) \times 10^{-12} \left(\frac{E}{777.1} \right)^{-(2.2+0.11)\log(E/777.1))} cm^{-2} s^{-1} MeV^{-1}$$

PKS 0625-354

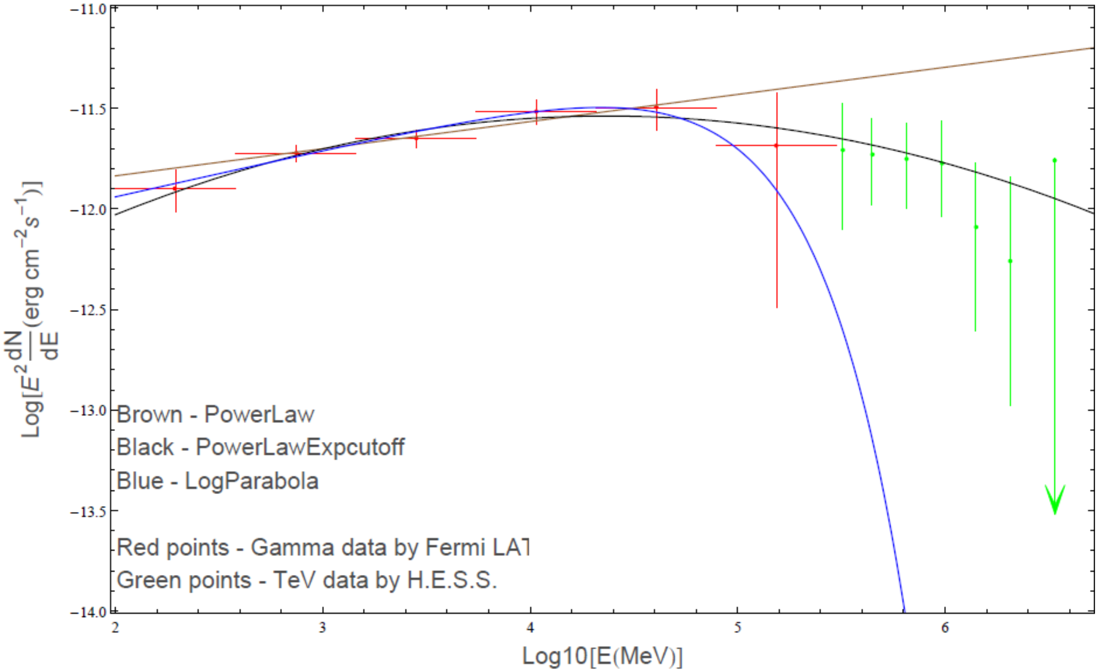

Power-Law

$$\frac{dN}{dE} = (2.5 \pm 0.1) \times 10^{-13} \left(\frac{E}{2382}\right)^{-1.86 \pm 0.04} cm^{-2} s^{-1} MeV^{-1}$$

The HESS spectrum can be explained when the Power-Law Exponential cut-off model is extrapolated to TeV energies.

$$\frac{dN}{dE} = (7.2 \pm 1.32) \times 10^{-11} \left(\frac{E}{100}\right)^{-1.77 \pm 0.06} \exp\left(-\frac{E}{94150}\right) cm^{-2} s^{-1} MeV^{-1}$$

Unusual spectrum

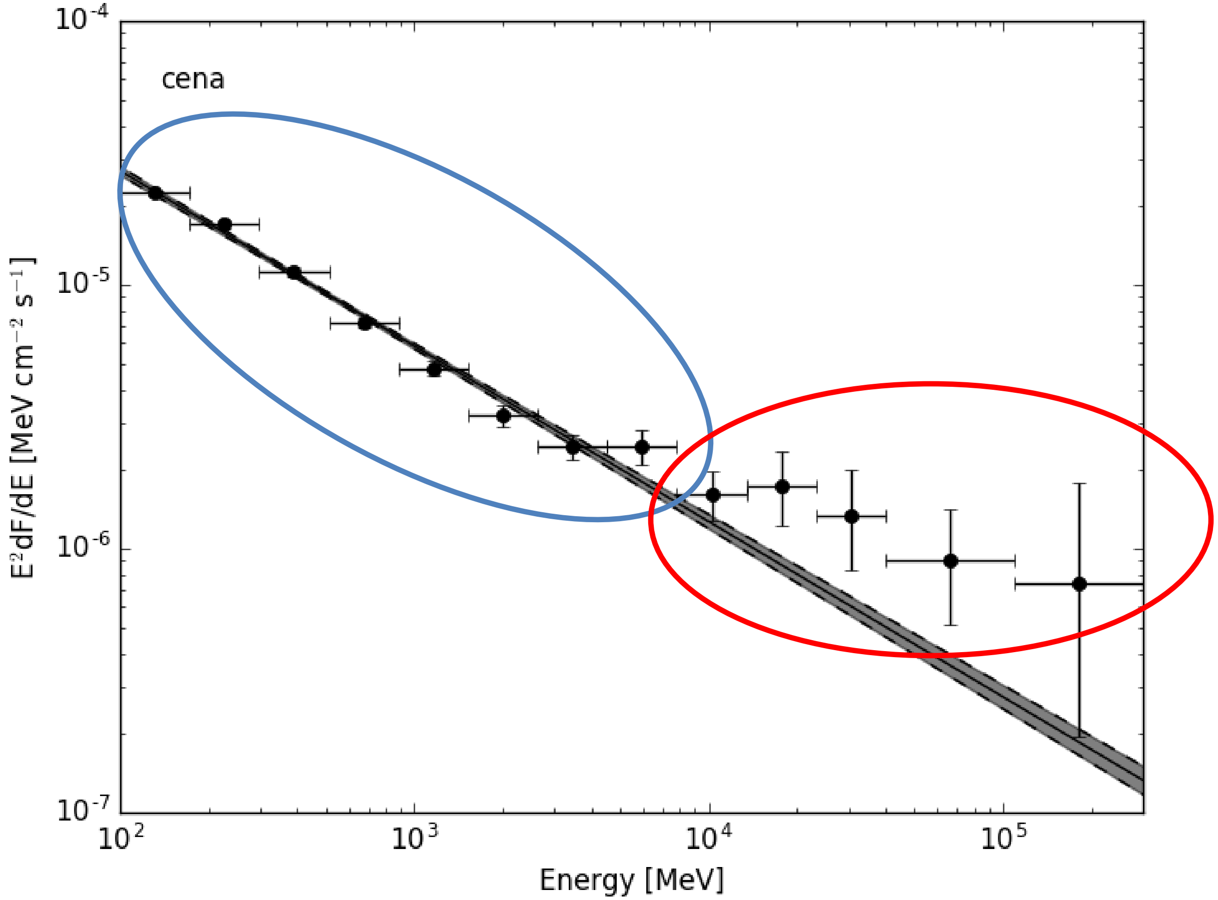

Variability

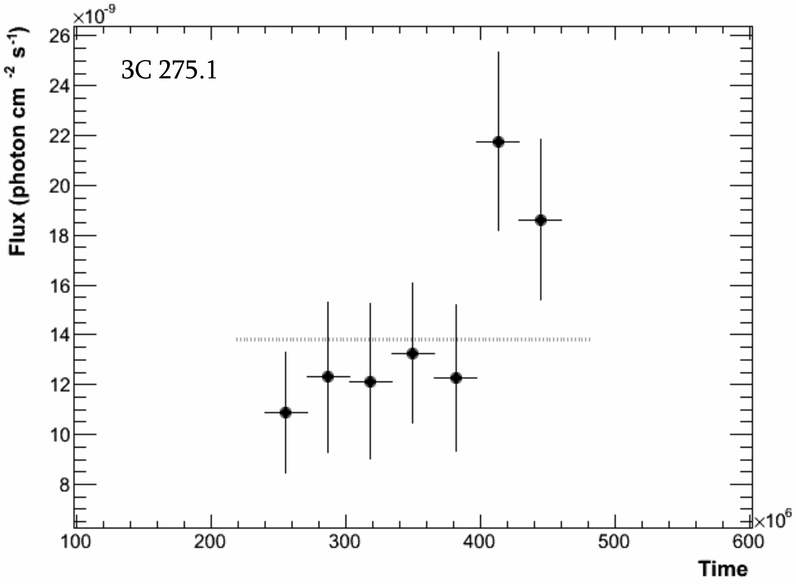

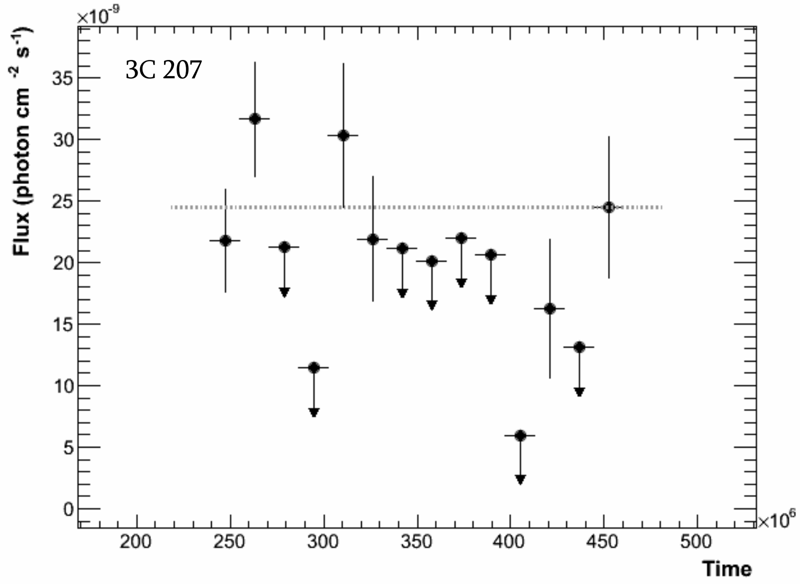

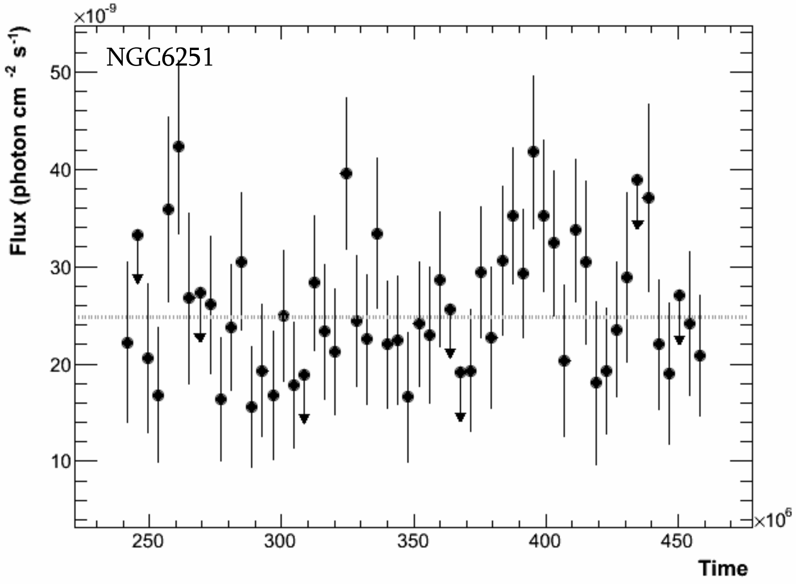

Variable Sources

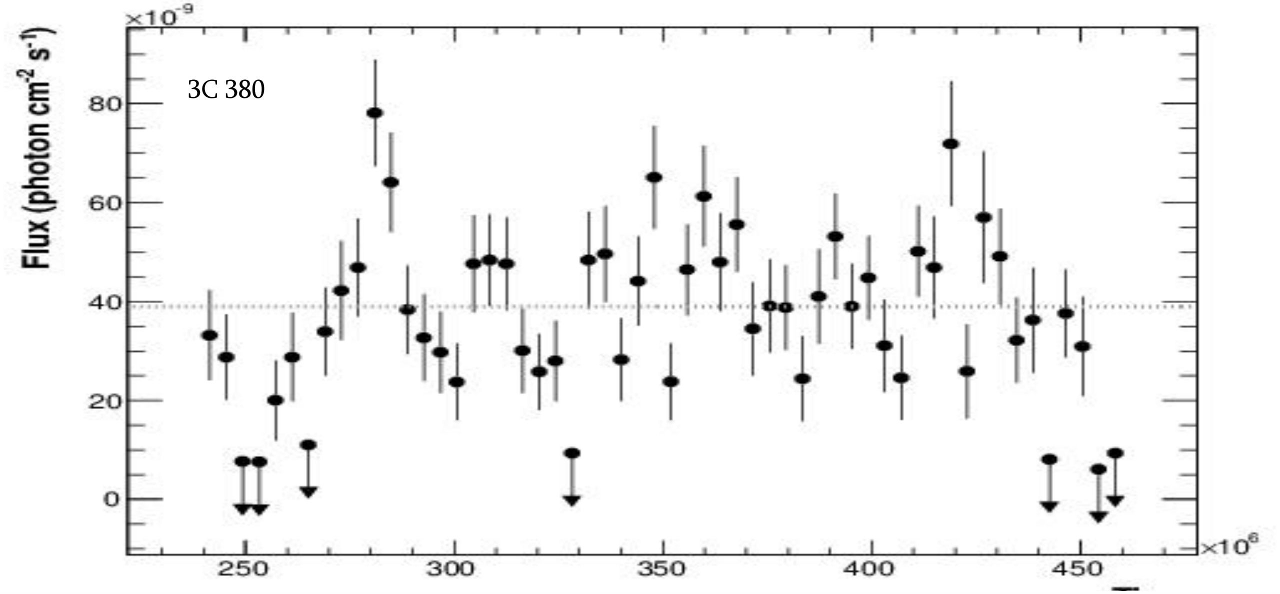

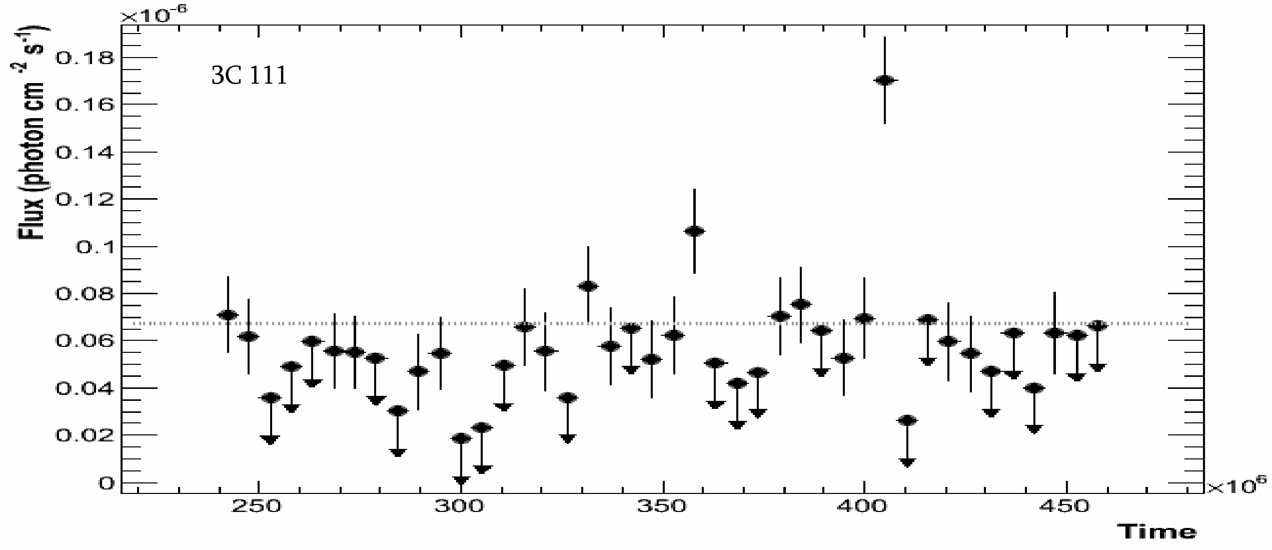

NGC 1275

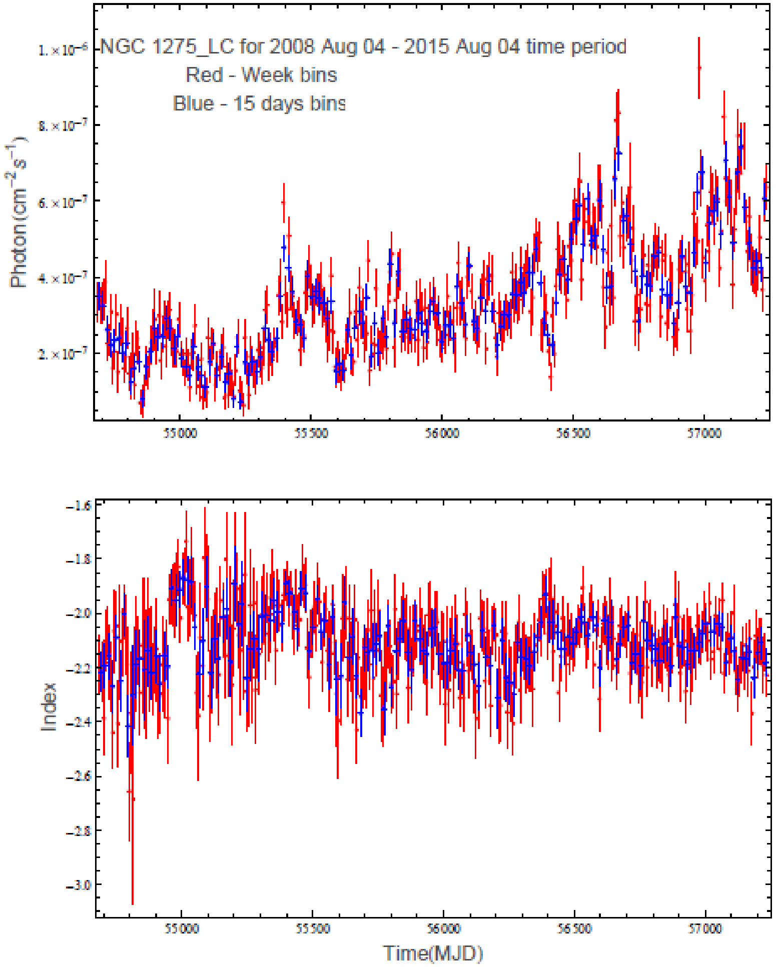
NGC 1275_LC for 2008 Aug 04 - 2015 Aug 04 time period
Red - Week bins
Blue - 15 days bins
Photon(cm^{-2}s^{-1})
Index
Time(MJD)

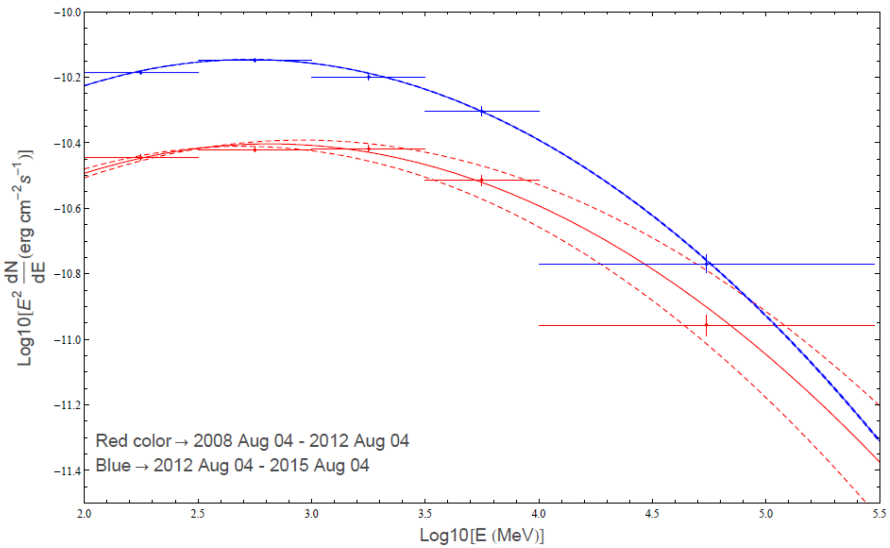
Log10[$E^2 \frac{dN}{dE}$(erg cm^{-2}s^{-1})]
Red color → 2008 Aug 04 - 2012 Aug 04
Blue → 2012 Aug 04 - 2015 Aug 04
Log10[E (MeV)]

Flare-Post Flare

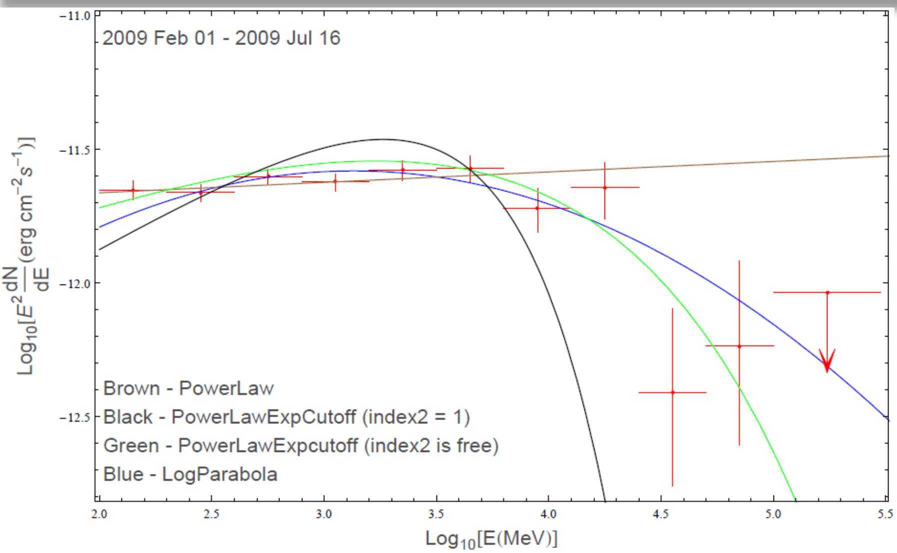

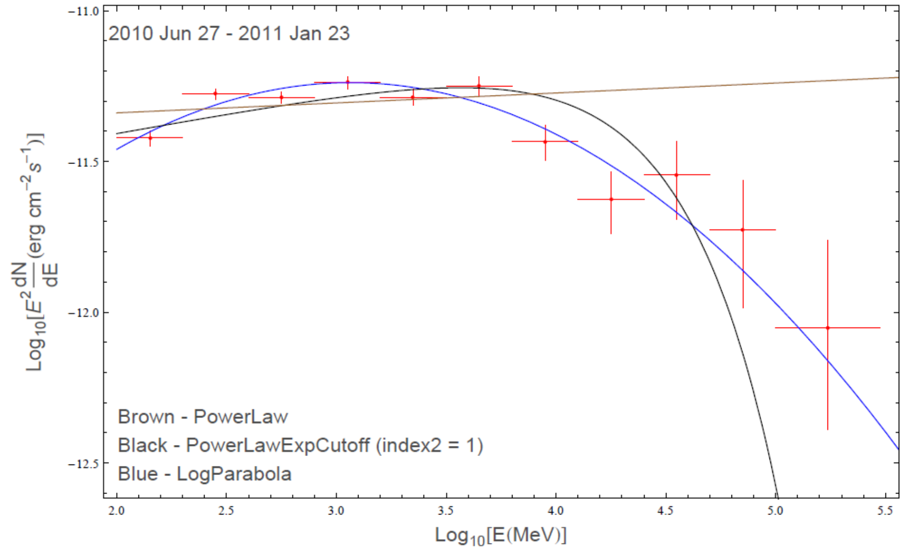

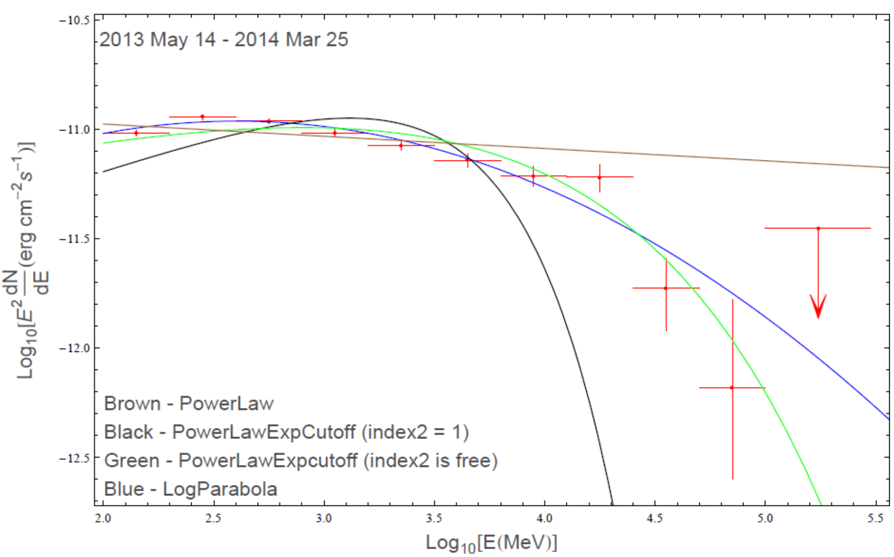

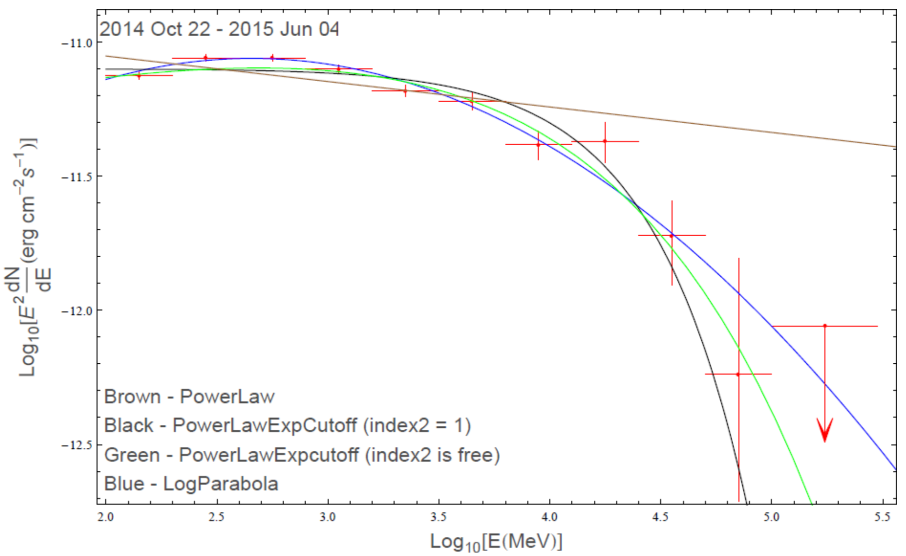

First Flaring period

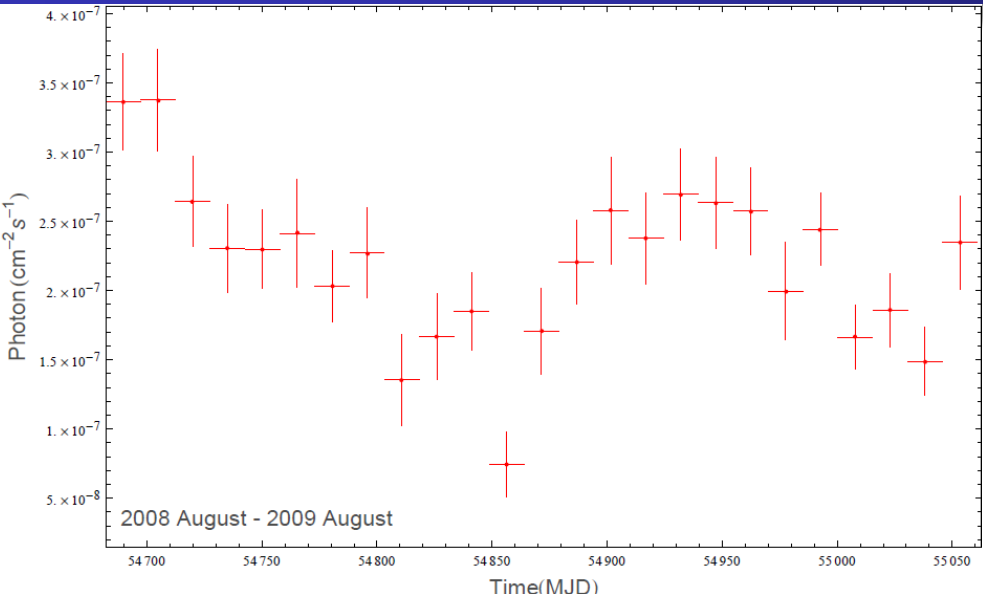

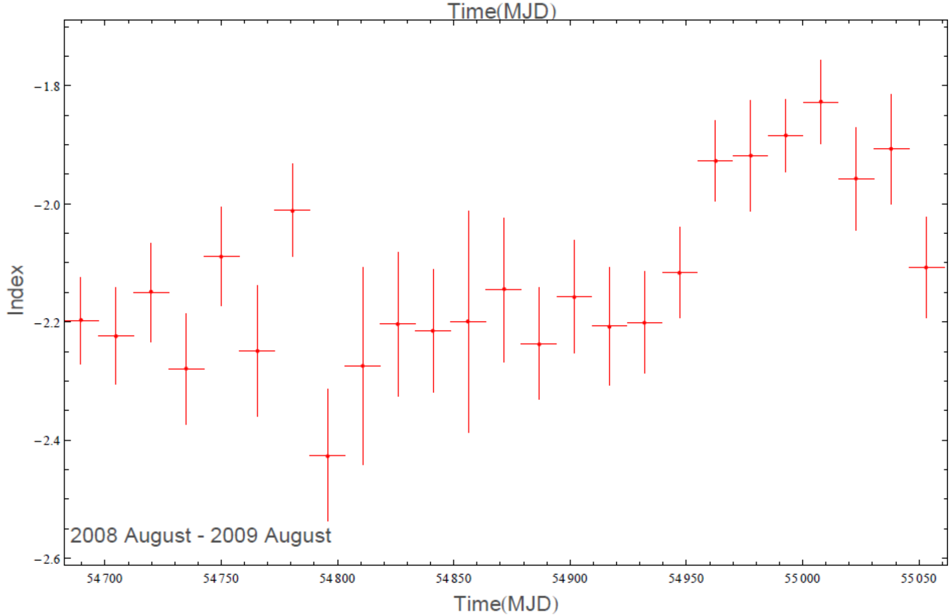

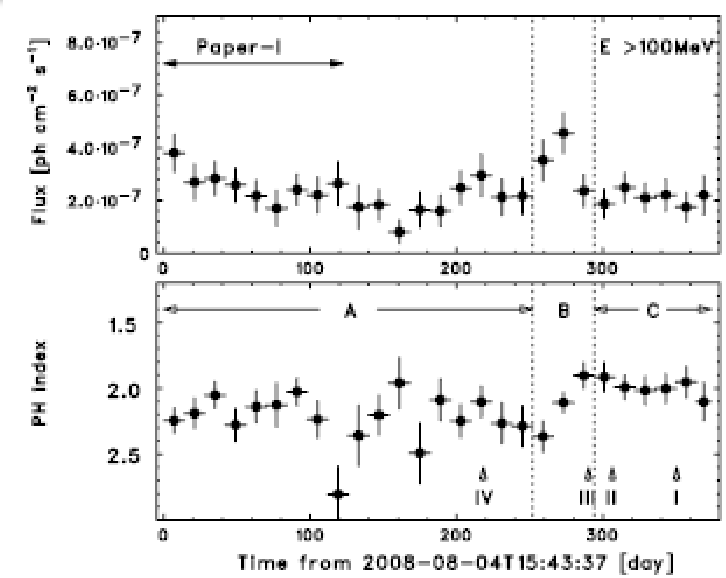

Kataoka et al. 2010

Index changes from 2.2 to <2.0

More detailed view

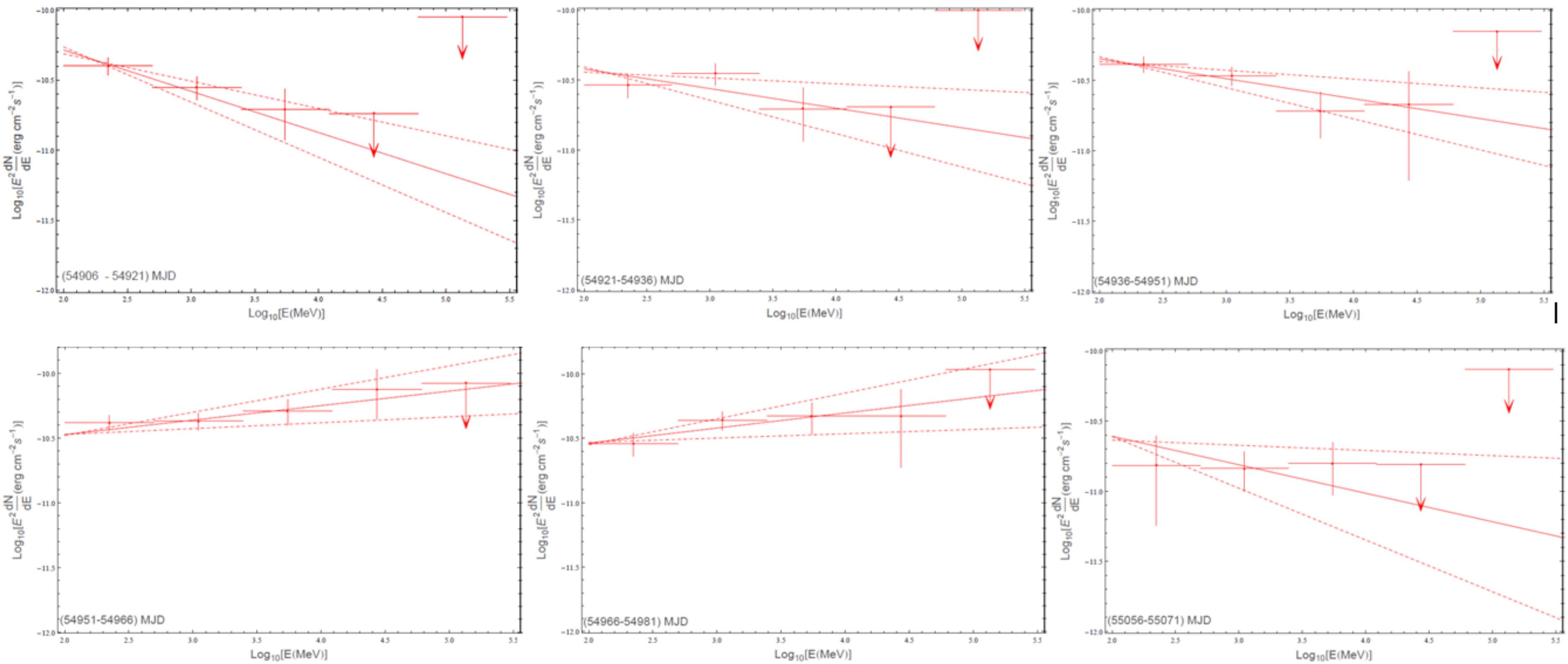

GB 1310+487

Gamma-ray/radio-loud narrow-line AGN at z = 0.638.

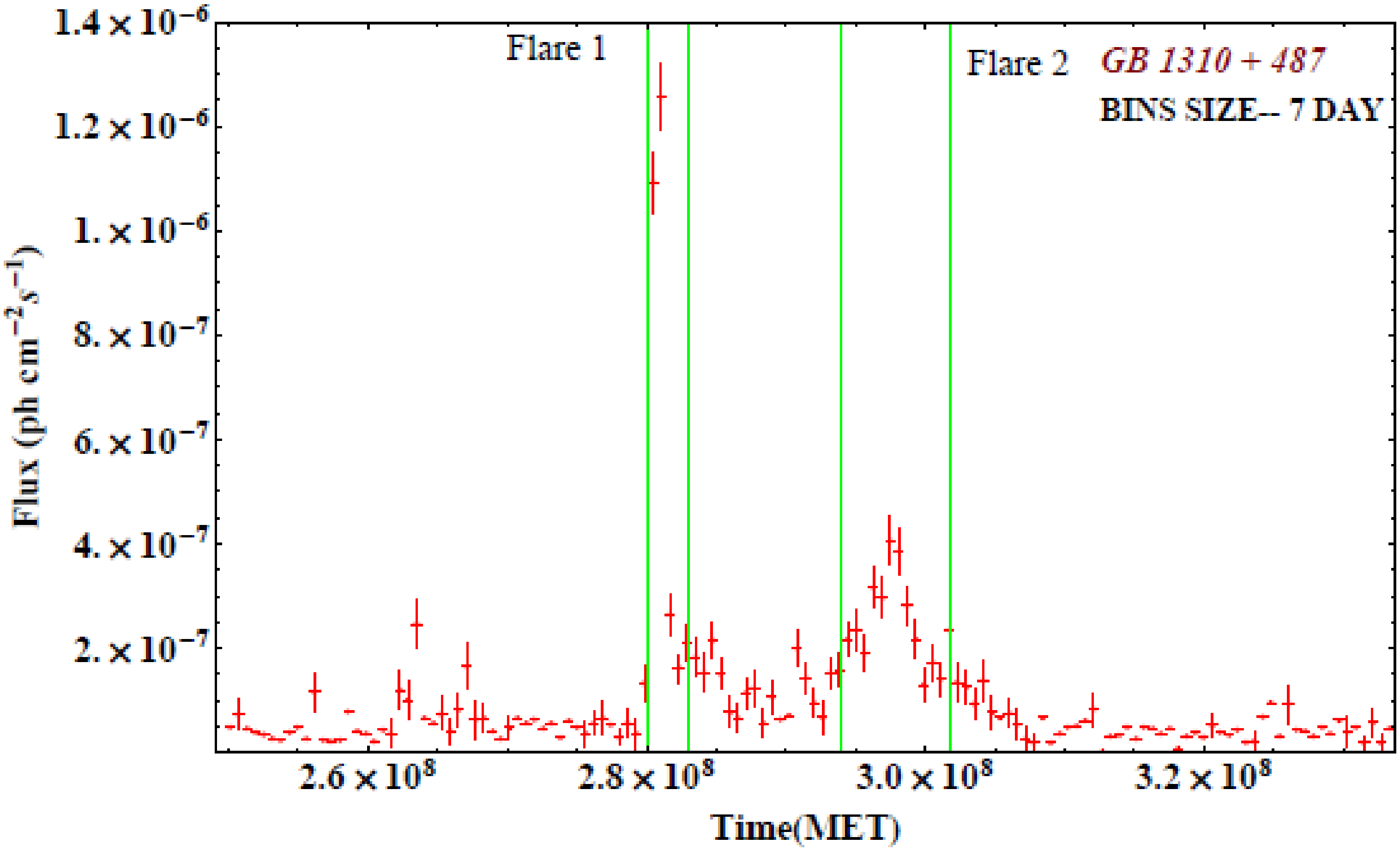

Flare -1 and Flare -2

Flare -1
2009-11-16—2009-12-21

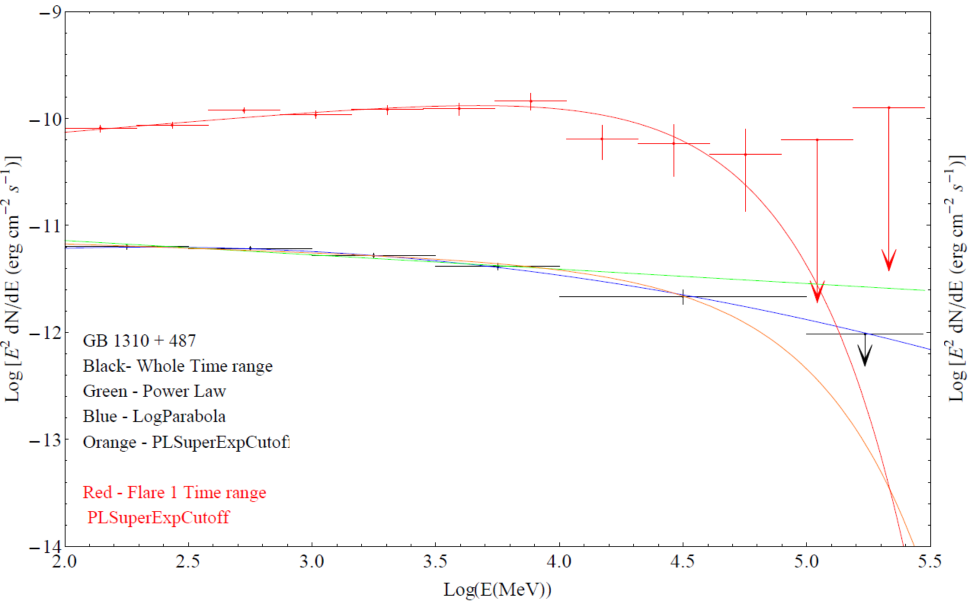

$$\frac{dN}{dE} = (3.8 \pm 0.2) \times 10^{-11} \left(\frac{E}{1446.36} \right)^{-1.8 \pm 0.04} \exp\left(-\left(\frac{E}{23491} \right) \right) cm^{-2} s^{-1} MeV^{-1}$$

Flare -2
2010-04-26—2010-07-26

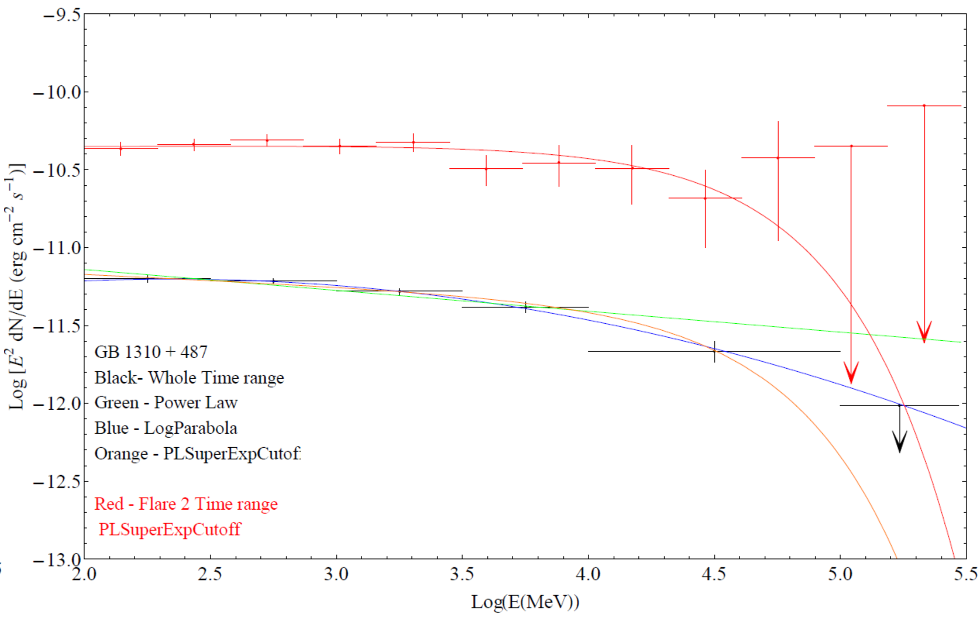

$$\frac{dN}{dE} = (1.36 + \pm 0.12) \times 10^{-11} \left(\frac{E}{1446.36} \right)^{-1.9 \pm 0.02} \exp\left(-\left(\frac{E}{46065} \right) \right) cm^{-2} s^{-1} MeV^{-1}$$

Luminosity-Photon index

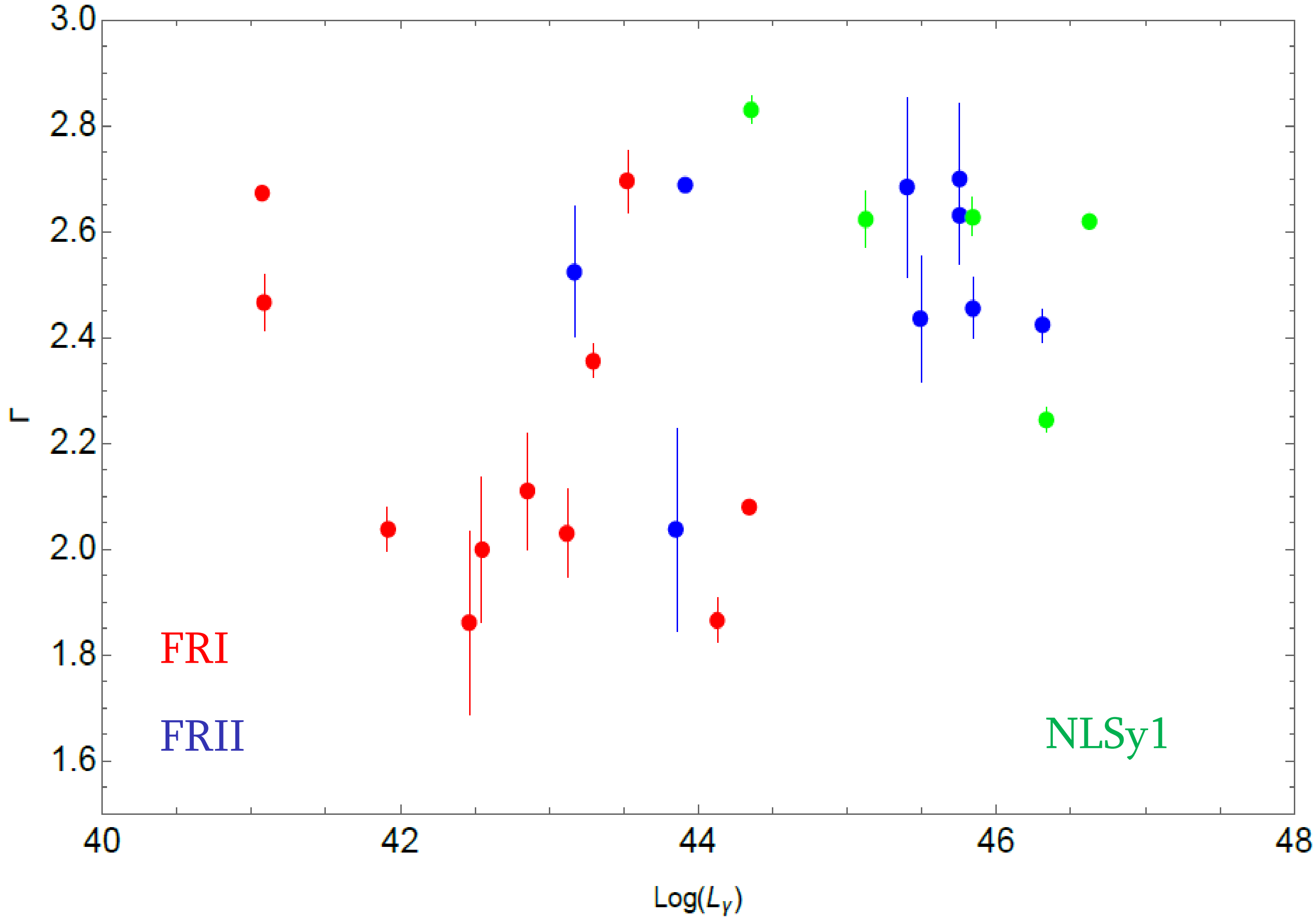

Individual Sources

Cen A core @ HE (4 year data)

Fermi LAT data from four years of observations of Cen A => detection of HE (>100 MeV) gamma-rays up to 50 GeV with detection significance of about 44 sigma

Sahakyan, Yang, Aharonian, and Rieger 2013 *ApJ*, 770, L6

The power-law fit with data:

$$\left(\frac{dN}{dE}\right)_p = (2.73 \pm 0.12) \times 10^{-9} \left(\frac{E}{100\,MeV}\right)^{-2.69 \pm 0.03}$$

The spectrum shows a tendency for a deviation from a single power law with respect to the data above several GeV.

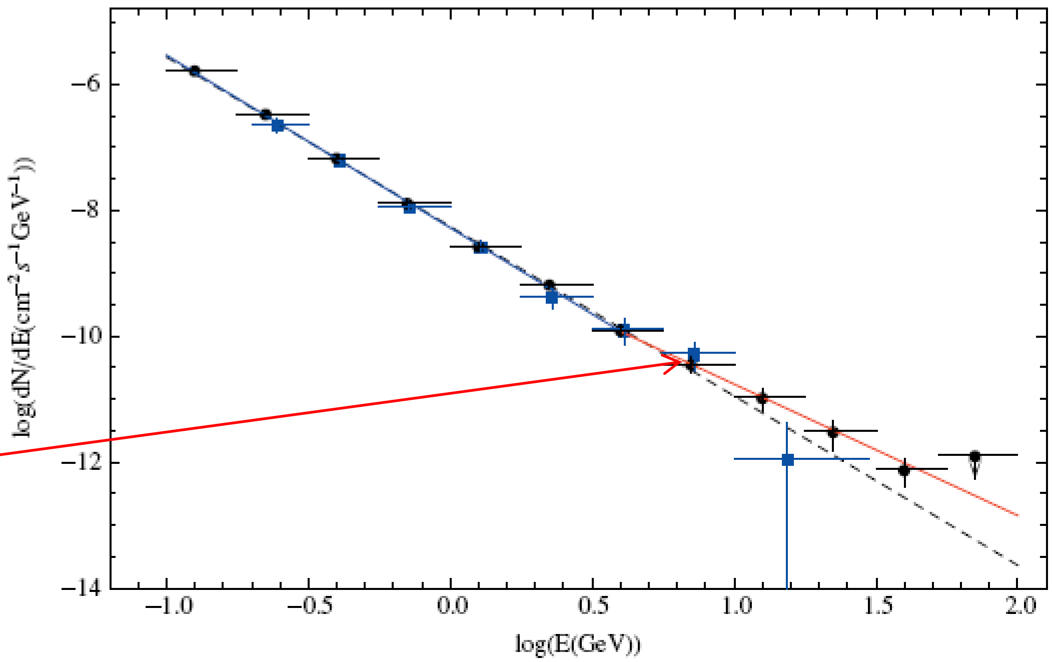

Broken power-law fit with data:

$$\left(\frac{dN}{dE}\right)_{bp} = (1.19 \pm 0.08) \times 10^{-13} \left(\frac{E}{4\,GeV}\right)^{-\Gamma_{1,2}}$$

with $\Gamma_1 = 2.74$ and $\Gamma_2 = 2.12$

The log likelihood ratio test givea preference to a broken power-law model.

Second Component ?

The results of the data analysis reveal a hardening of the (average) gamma-ray core spectrum toward higher energies. The "unusual" break at 4 GeV could most naturally be explained by a superposition of different spectral components.

The power-law fit in the range 0.1-4 GeV

photon index - $\Gamma_1 = 2.74 \pm 0.02$

flux - $F_\gamma = (1.68 \pm 0.04) \times 10^{-7}\, ph\, cm^{-2} s^{-1}$

detection significance - $TS = 1944$

The power-law fit in the range 4-100 GeV

photon index - $\Gamma_2 = 2.09 \pm 0.2$

Flux - $F_\gamma = (4.2 \pm 0.64) \times 10^{-10}\, ph\, cm^{-2} s^{-1}$

detection significance- $TS = 124.4$

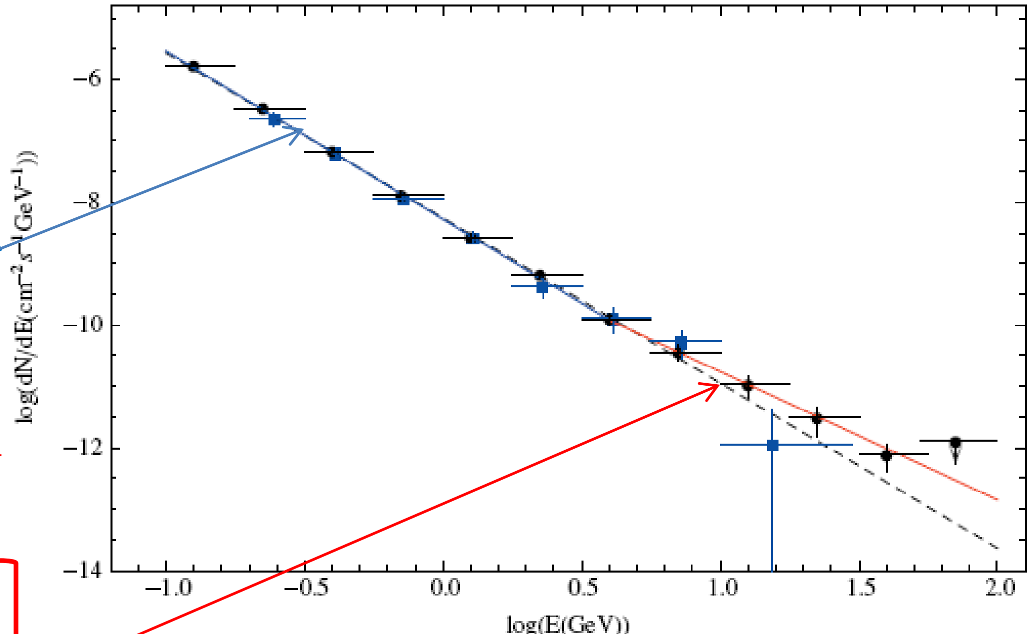

Sahakyan, Yang, Aharonian, and Rieger 2013 *ApJ*, 770, L6

hardening of the spectrum !

Time variability

Time variability $\Rightarrow$ region size

$$R \leq \frac{\delta_D}{1+z} c t_{\mathrm{var}} \, cm$$

Low Energy Component

45 day bin

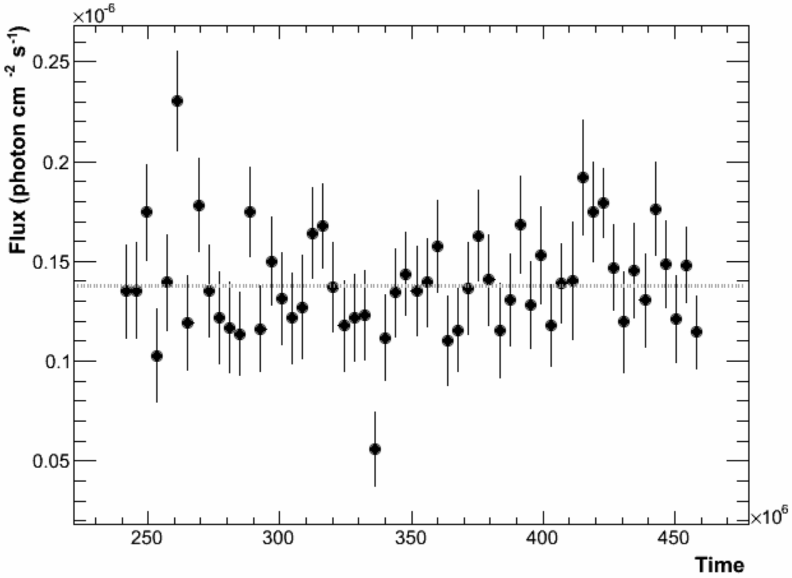

High Energy Component

90 day bin

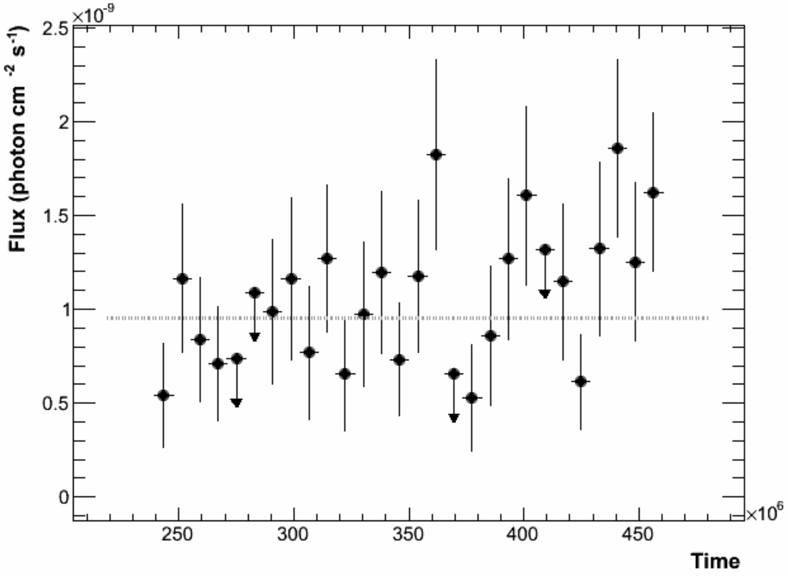

Spectral Energy Distribution

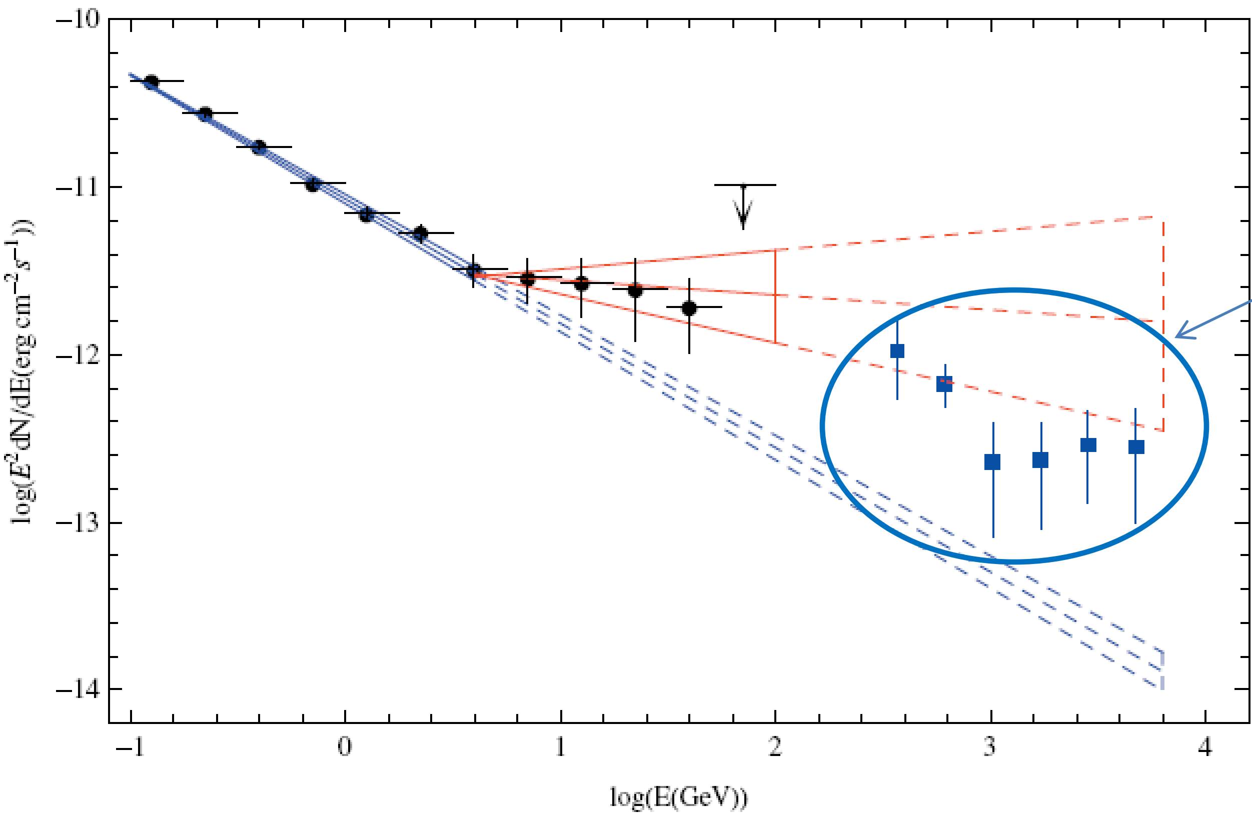

HESS data
Aharonian et al. 2009

For a distance of 3.8 Mpc, corresponds to apparent (isotropic) gamma-ray luminosities: $L_\gamma(0.1-4\,GeV) \approx 10^{41}\,erg\,s^{-1}$ and $L_\gamma(>4\,GeV) \approx 1.4\times10^{40}\,erg\,s^{-1}$ which are larger than VHE luminosity reported by HESS $L_\gamma(>250\,GeV) \approx 2.6\times10^{39}\,erg\,s^{-1}$ Aharonian et al. 2009, ApJ, 695, L40

Origin of HE and VHE gamma-rays

The lack of significant variability + limited angular resolution (~5 kpc)-> uncertainties production site of the HE gamma-ray emission.
In terms of SSC processes occurring in inner jet-> well modeling up to a few GeV (e.g., Chiaberge et al. 2001; Abdo et al. 2010). However the hardening on the HE spectrum above 4 GeV -> appearance of a physically different component.
Different scenarios for new additional component:

(1) non-thermal processes in its BH magnetosphere (Rieger & Aharonian 2009),
(2) multiple SSC-emitting components (i.e., differential beaming; Lenain et al. 2008),
(3) photo–meson interactions of protons in the inner jet (Kachelrieß et al. 2010; Sahu et al.2012),
(4) gamma-ray-induced pair-cascades in a torus-like region (Roustazadeh & Bottcher 2011),
(5) secondary Compton upscattering of host galaxy starlight (Stawarz et al. 2006),
(6) inverse-Compton processes in the kpc-scale jet (Hardcastle & Croston 2011).

Also gamma-rays can be produced from relativistic protons. Effective gamma-ray production if the diffusion coefficient does not exceed $D \sim R_h^2 / t_{pp} \sim 10^{28} (R_h / 10\,kpc)^2 (10^{-2}\,cm^{-3}/n) cm^2 s^{-1}$ by much. An interesting possibility, especially for the hard HE component with photon index close to 2.1, given the similarity to so-called "Fermi Bubbles".

Cen A lobes @ HE- 10 month data

After 10 months Fermi LAT operation discovery of the HE gamma-ray emission from radio lob

Count map

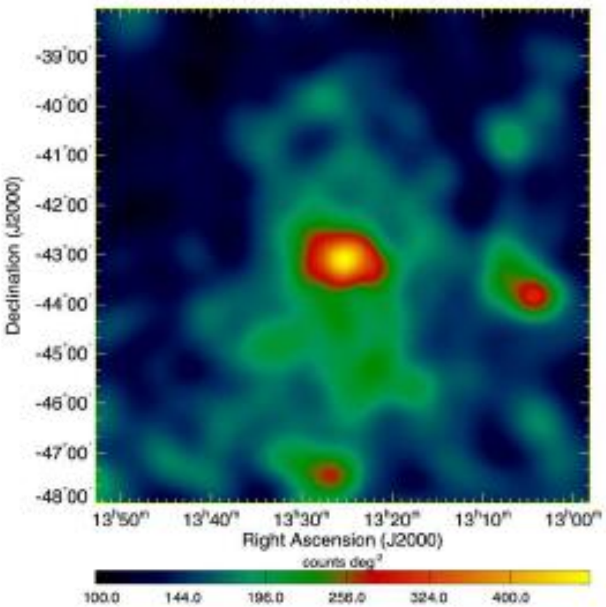

SED

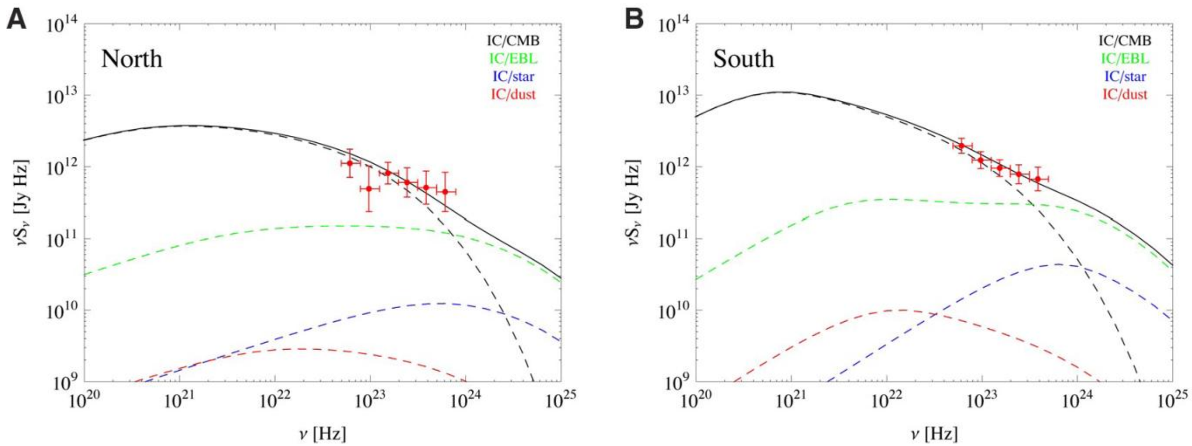

N lobe- $F_\gamma = 0.77 \times 10^{-7}\, ph\, cm^{-2}\, s^{-1}$

S lobe- $F_\gamma = 1.09 \times 10^{-7}\, ph\, cm^{-2}\, s^{-1}$

With photon index $\Gamma \approx 2.6$

Gamma-rays are the result of IC scattering of cosmic microwave background photons and the extragalactic background light photons by *in situ accelerated* electrons

Fermi-LAT Collaboration, Science , 2010, 328, 725.

Cen A lobes @ (3 year data)

3 times larger than the previous observation -> study the morphology and photon spectrum with higher statistics.

1) detected >10 sigma up to 6 GeV
2) photon index -2.6 for Southern, harder for Northern -2.24
3) substantial extension of HE emission beyond radio/ WMAP for Northern part
4) HE gives model-independent info about spatial distribution of electrons

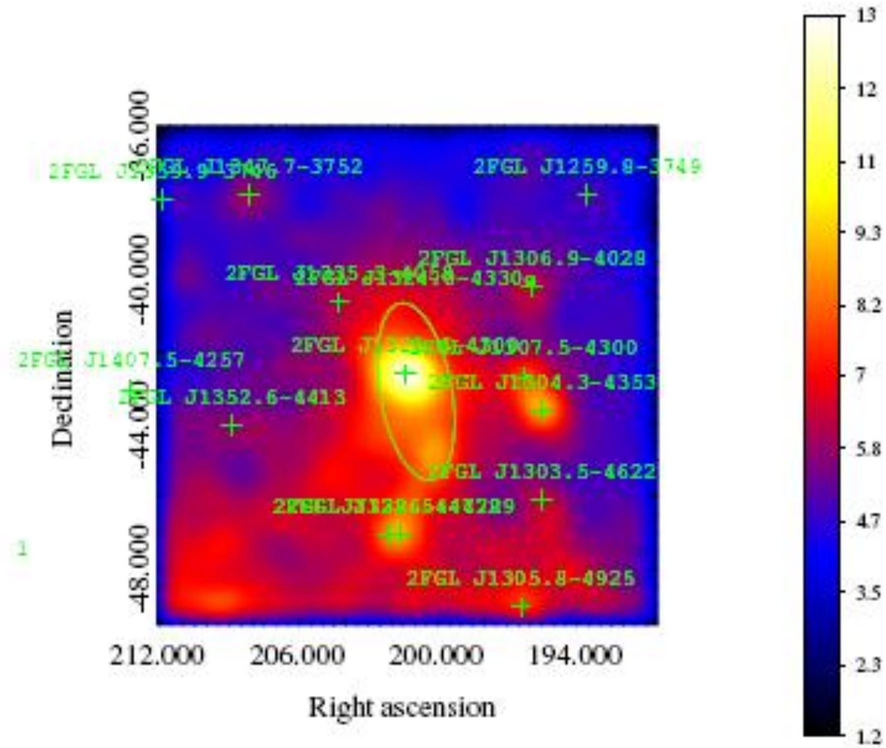

Yang , Sahakyan + Rieger A&A, 2012, 542, A19

Spatial distribution of electrons

The radio luminosity depends on electron density N_e and magnetic-field square B^2. The IC gamma-ray luminosity only depends on N_e -> only HE gamma-rays can give model-independent information about both the energy and spatial distribution of electrons

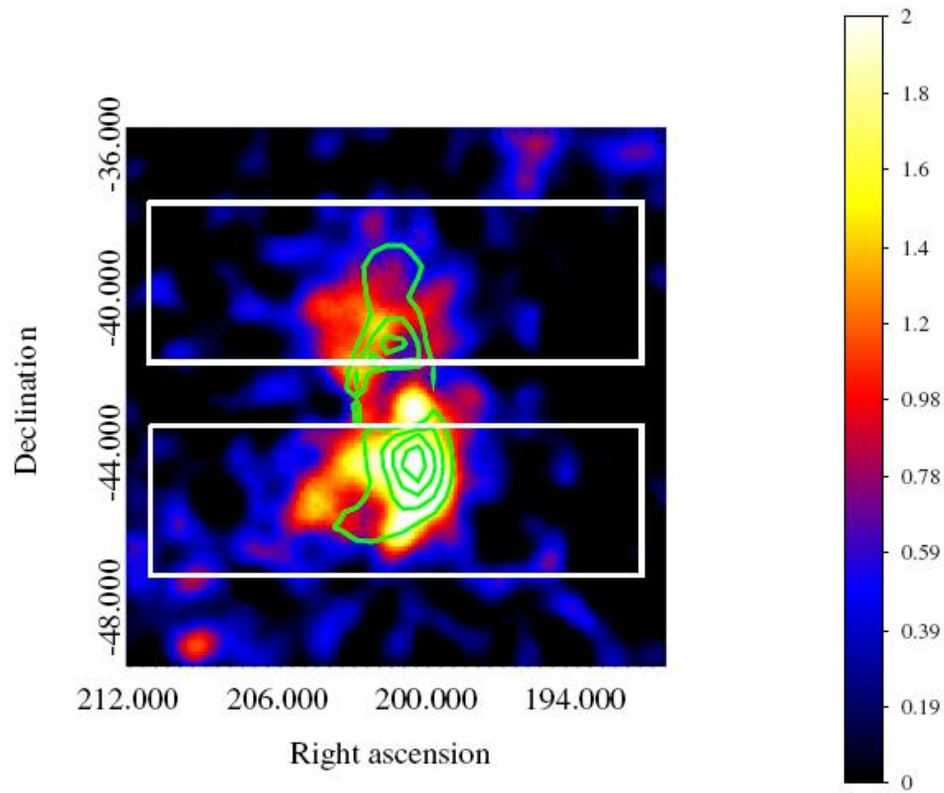

(b) Excess map after background subtraction.

Extension of HE emission observed for Cen A Northern lobe -> example showing no conclusions can be made about electron density based on radio observations !

Yang , Sahakyan + Rieger A&A, 2012, 542, A19

Origin of gamma rays

Leptonic origin:

radio emission $\Longrightarrow$ nonthermal / synchrotron radiation existence of multi-GeV electrons $\Longrightarrow$ photons scattering due to IC on different target photon field.

i) CMB photon field – main contribution

ii) EBL photon field – some contribution (for highest γ energies)

iii) Synchrotron photon field – negligible

Hadronic origin:

protons can interact with the ambient low density plasma, creating daughter mesons and neutral component decay into γ-rays $p + p \Rightarrow \pi^0 \Rightarrow \gamma\gamma$

Electron spectrum

The general equation describing evolution of energy distribution function ***f*** of relativistic particles can be written as

$$\frac{\partial f}{\partial t} = div(D_r grad\, f) - div(u_r\, f) + \frac{\partial (P_r f)}{\partial \gamma} - \frac{\partial (b_r f)}{\partial \gamma} + \frac{\partial^2 (d_r f)}{\partial \gamma^2}$$

P_r is the energy loss rate, D_r is the diffusion coefficient, u_r is the fluid velocity and b_r and d_r are acceleration efficiencies. After integration by volume

$$\frac{\partial N}{\partial t} = \frac{\partial}{\partial \gamma}(PN) - \frac{N}{\tau_{esc}} + Q$$

where $N(\gamma,t)$ is electron energy distribution function , τ_{esc} is escape time and $Q(\gamma,t)$ is the injection rate of electrons. The solution of kinetic equation is

$$N(\gamma,t) = \frac{1}{P(\gamma)} \int_{-\infty}^{t} P(\zeta_t) Q(\zeta_t, t_1) e^{-\int_{t_1}^{t} \frac{dx}{\tau(\zeta_x)}} dt_1$$

Escape of particles from the lobes

The particles can escape from the lobes only by diffusion $\tau_{esc} = \frac{R^2}{2D(E)}$

where $D(E)$ is the diffusion coefficient and generally is taken in the form

$$D(E) = \eta \frac{r_g c}{3}$$

$r_g = 3.3 \times 10^{13} (\frac{E}{10\,GeV})(\frac{B}{1\,\mu G})^{-1}\, cm$ is the particle gyroradius and η is the gyrofactor.

The electrons lose energy mainly by IC cooling

$$t_{cooling} = 1.24 \times 10^8\, E^{-1}{}_{10GeV}\, yr$$

the escape distance is

$$t_{cooling} = \tau_{esc} \Rightarrow \qquad R = 16.6\, B_{1\mu G}^{-1/2} \eta^{1/2}\, pc$$

which is very small compared to the size of the outer lobes of Cen A (250 kpc) $\Rightarrow$

$N(\gamma,t) = \frac{1}{P(\gamma)} \int_{\gamma}^{\xi(t)} Q(\gamma_1) d\gamma_1$ where $t = \int_{\gamma}^{\xi(t)} \frac{d\gamma_2}{P(\gamma_2)}$ and $P(\gamma)$ is energy loss rate of electrons

Origin of gamma-rays

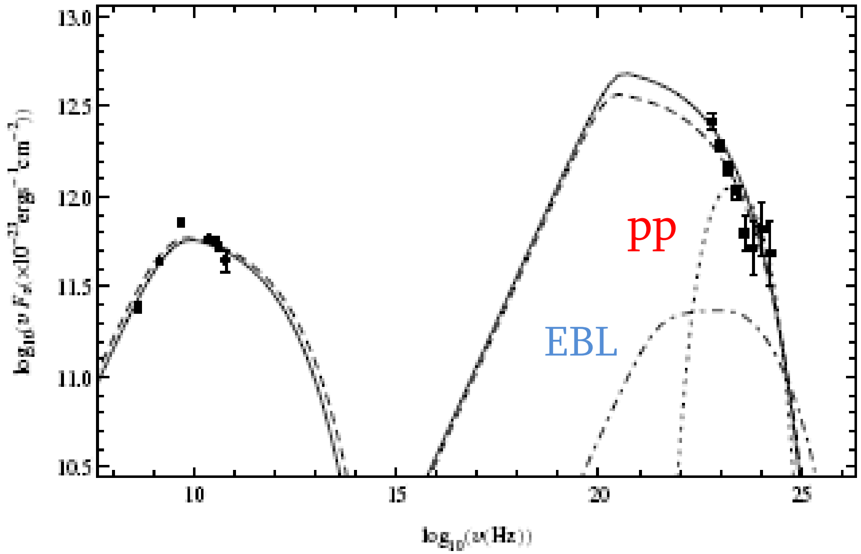

(a) South lobe

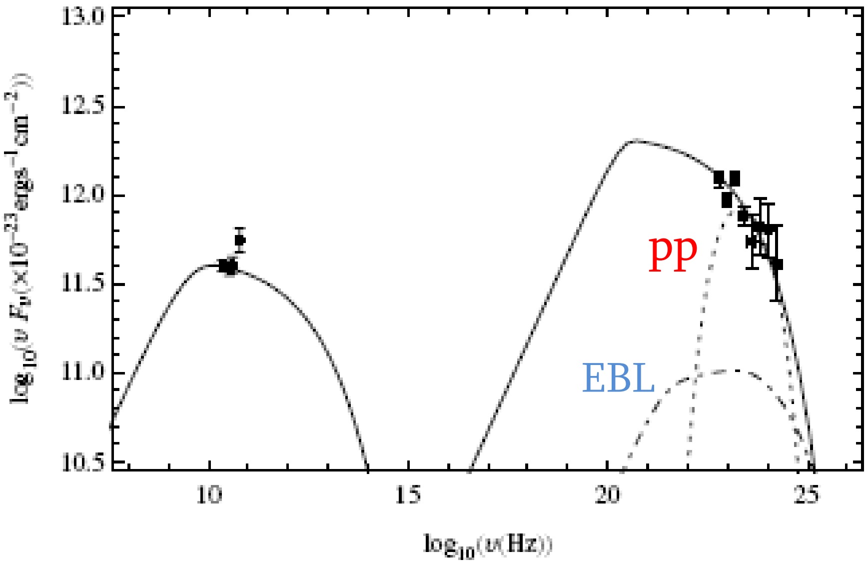

(b) γ-ray excess (lobe) region in the north

Leptonic gamma-rays

Synchrotron emission and IC scattering of electrons for injection $t = 8\times10^{7}\ yr$ and $\gamma_{max} = 10^{6}$. The maximum total energy of leptons

$$W_e = 6\times10^{57} erg$$

Hadronic gamma-rays

For $E_{p\max} = 55 GeV$ the maximum energy of hadrons

$$W_p = 10^{61}(n/10^{-4} cm^{-3})^{-1} erg$$

Yang , Sahakyan + Rieger A&A, 2012, 542, A19

Fornax A

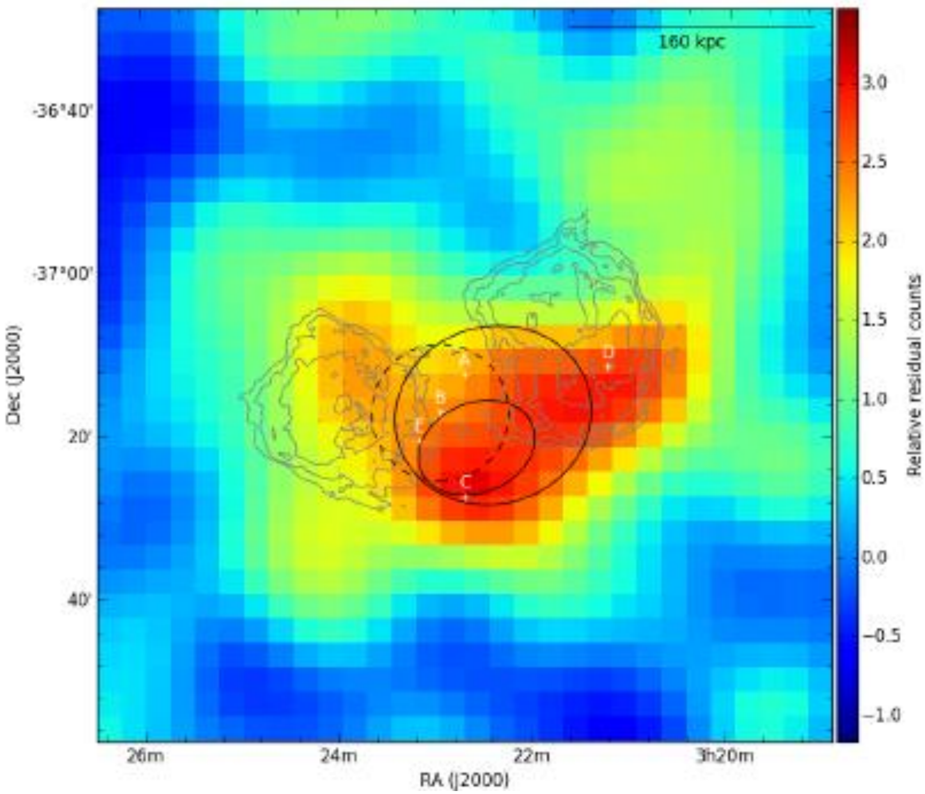

Ackerman, Ajelo and et al. 2016

Distance- 18.6 Mpc
Lobe size- 389 kpc

6.1 years
2008 August 4 2014 September 4

Detection significance: TS=121≈11 σ

The spectrum: Γ=2.08±0.08

Flux: $(5.34 \pm 0.78) \times 10^{-12}\ erg\ cm^{-2} s^{-1}$

Observation in the other waveband

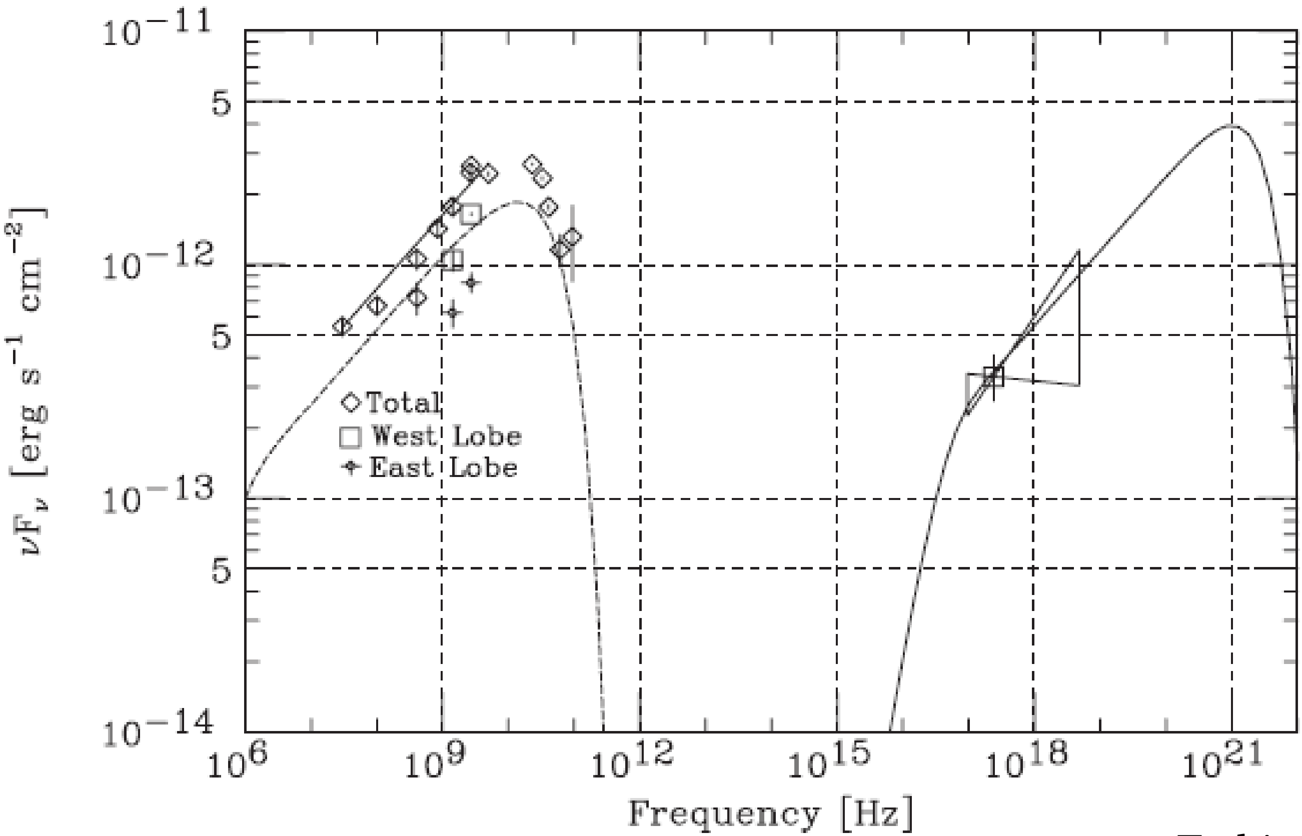

Tashiro et al. 2009

Radio photon index: Γ=1.68
X-ray photon index: Γ=1.62

The same population of electrons is responsible for radio (synchrotron) and X-ray (IC/CMB) emissions.

IC scattering of EBL photons

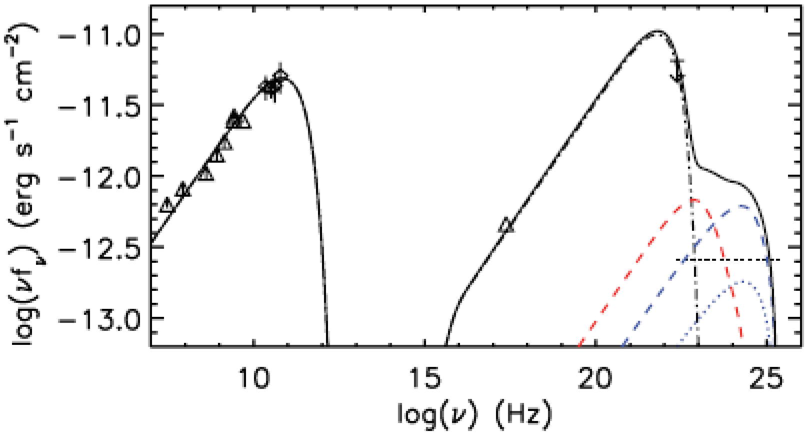

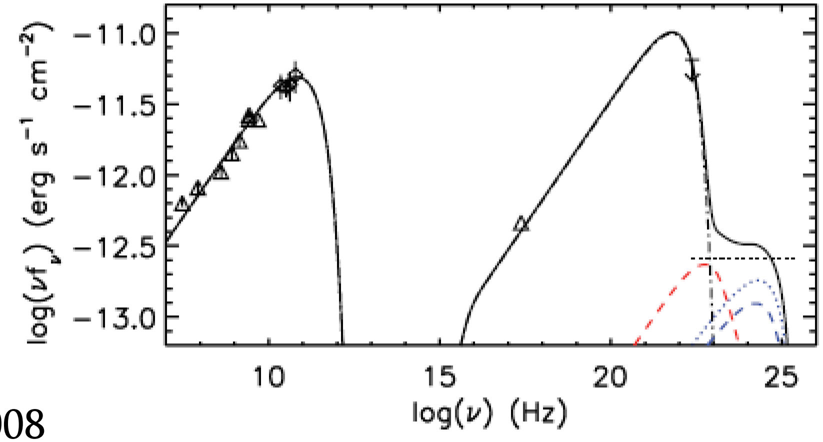

Georganopoulos et. al., 2008

The exact measurement of gamma-ray flux will allow to measure the EBL.

Overall SED

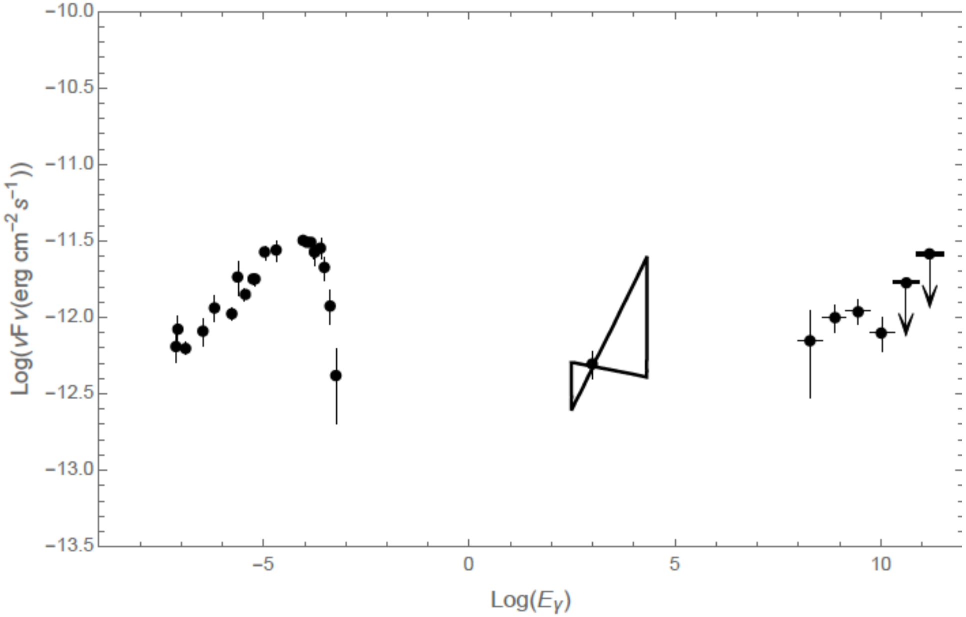

The multi-wavelength spectrum allows self-consistent estimation of the parameters describing the particle distribution.

$$N_e(E_e) = N_0 E_e^{-\alpha} Exp\left(-\left(\frac{E_e}{E_c}\right)^{\beta}\right) \qquad N_e(E_e) = N_0 \begin{cases} Ee^{-\alpha 1} & E_e < E_{br} \\ Ee^{-\alpha 2} & E_e > E_{br} \end{cases}$$

Derive the best-fit and uncertainty distributions of spectral model parameters through Markov Chain Monte Carlo sampling of their likelihood distributions

Leptonic

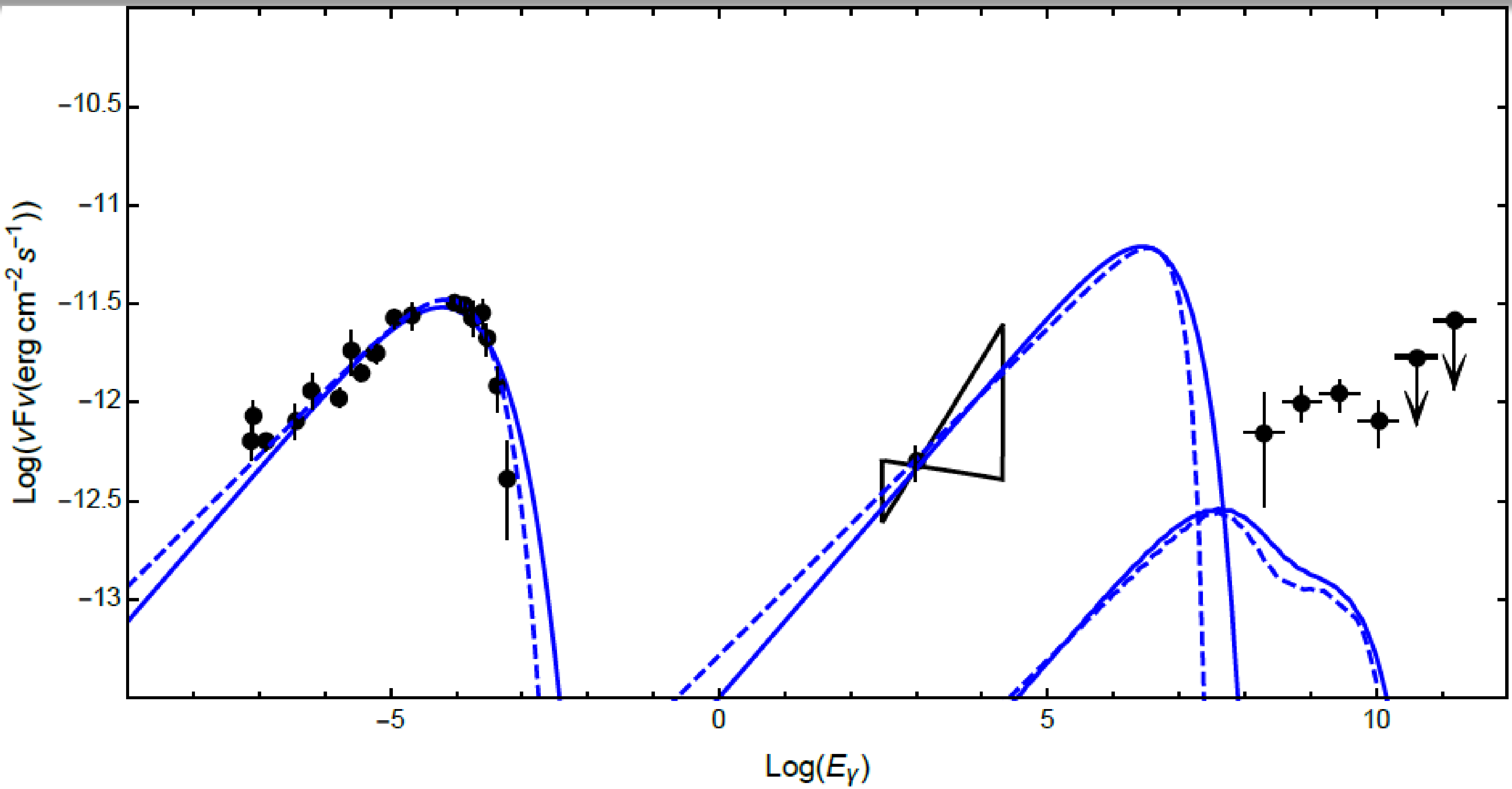

$$N_e(E_e) \propto N_0 E_e^{-\alpha} Exp\left(-\left(\frac{E_e}{E_c}\right)^2\right)$$

$$N_e(E_e) \propto N_0 E_e^{-\alpha} Exp\left(-\left(\frac{E_e}{E_c}\right)^7\right)$$

Several Maxwellian

The total electron spectrum is formed from the contribution of several relativistic Maxwellian distributions

$$n(\gamma) = n_0\, \gamma^2 e^{-\left(\frac{\gamma}{\gamma_c}\right)^\beta} \qquad \gamma_{ci} = (\gamma_1, \gamma_2 \ldots\ldots\gamma_i) \qquad W_i \propto \frac{1}{\gamma_{ci}{}^4}$$

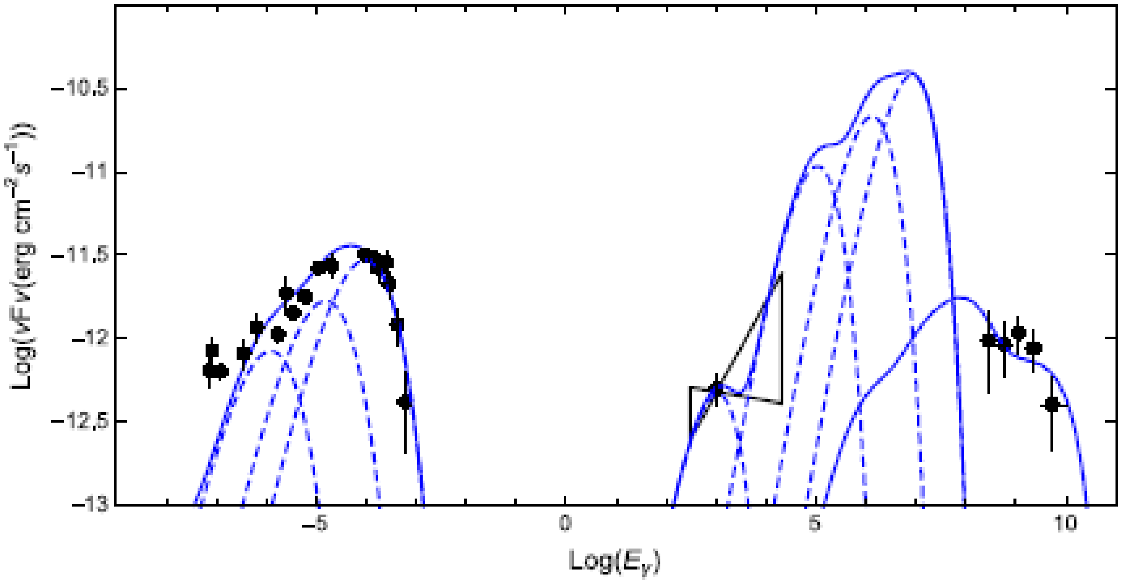

Lepto Hadronic scenario

The low energy emission produced from synchrotron emission of electrons, X-ray Emission from the IC scattering of CMB photons on the same electrons. The gamma-ray emission produced from the interaction of protons.

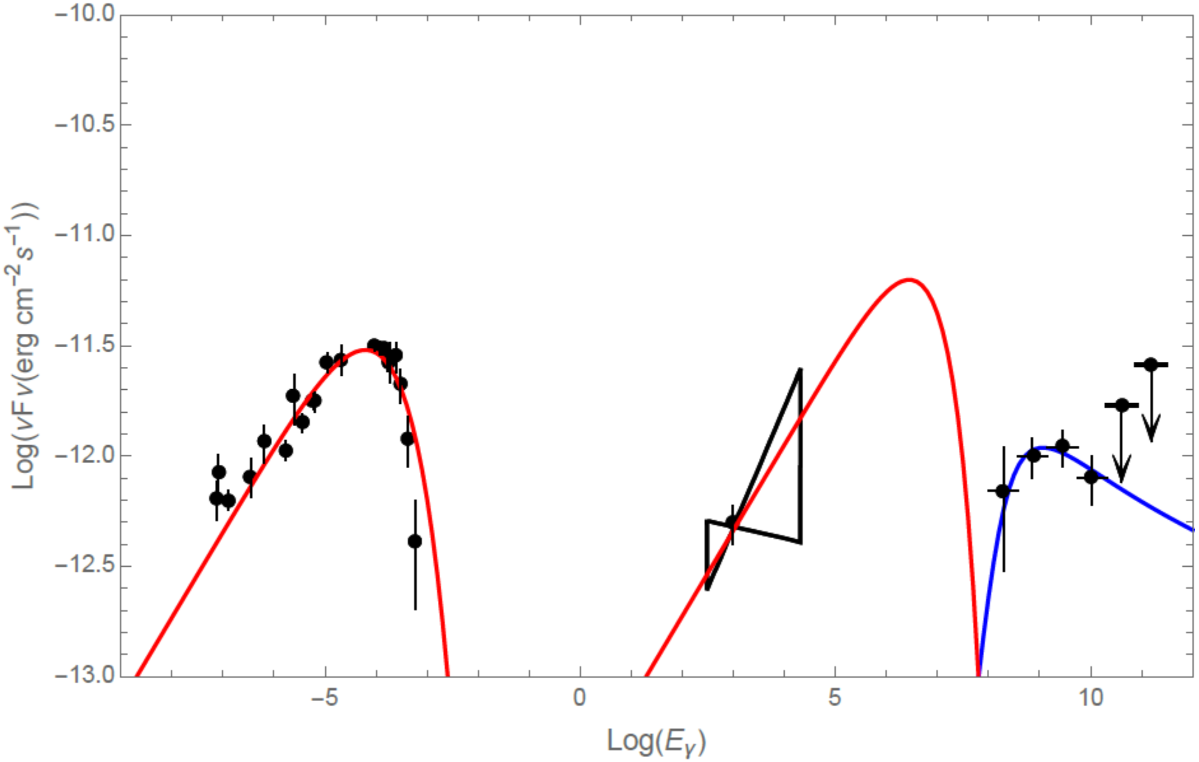

Emission from the compact regions

3C 120 radio galaxy at the redshift z=0.033 is an active and powerful emitter of radiation at all the observed wavebands

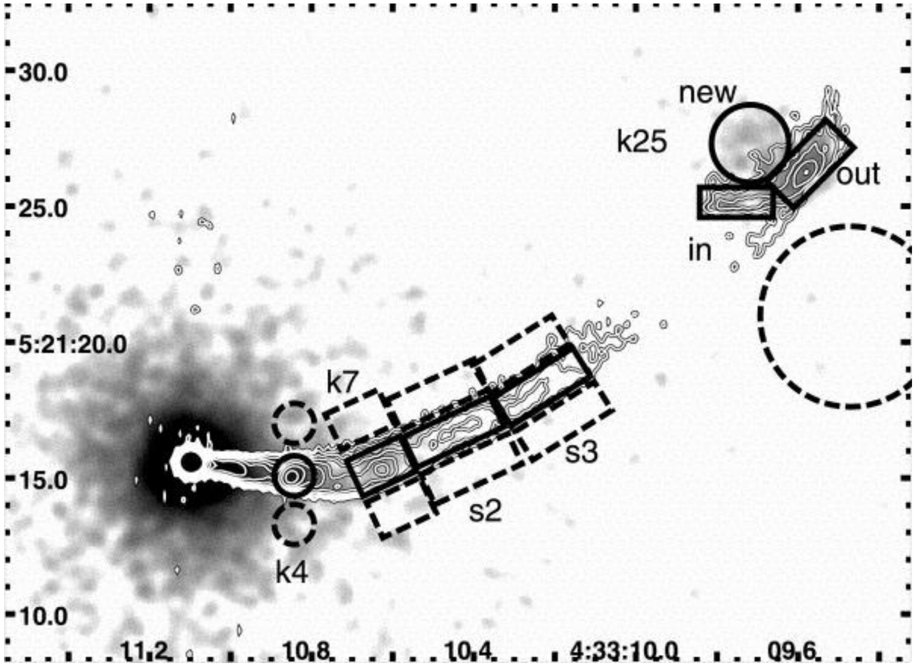

Harris et al. (2004)

Large Scale jet up to 100 kpc with several knots.

Emission from the knots

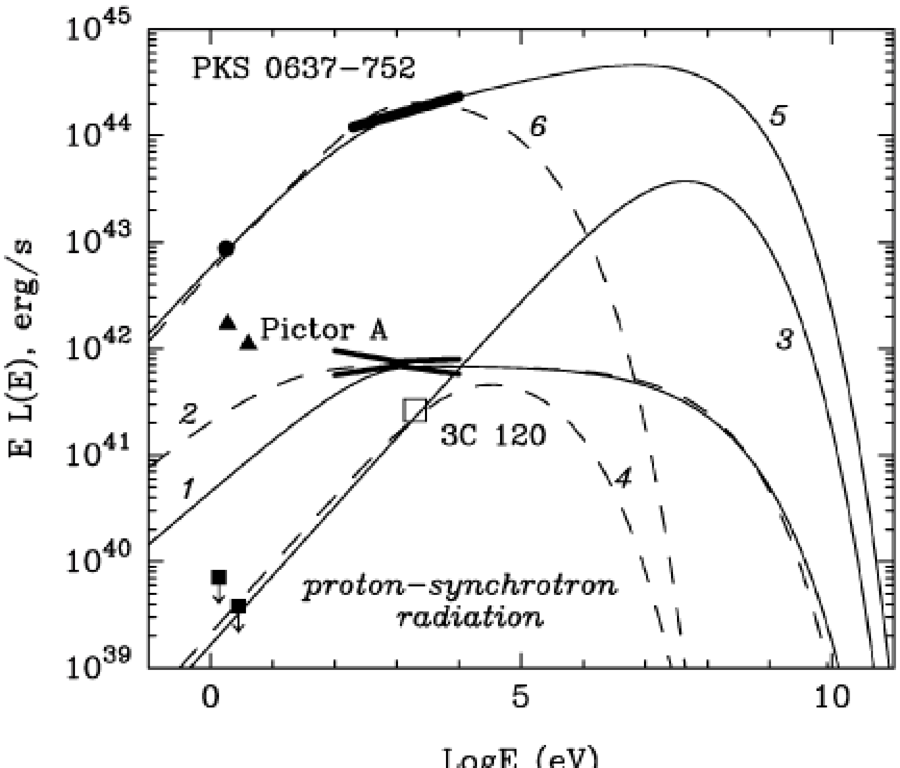

Aharonian 2002

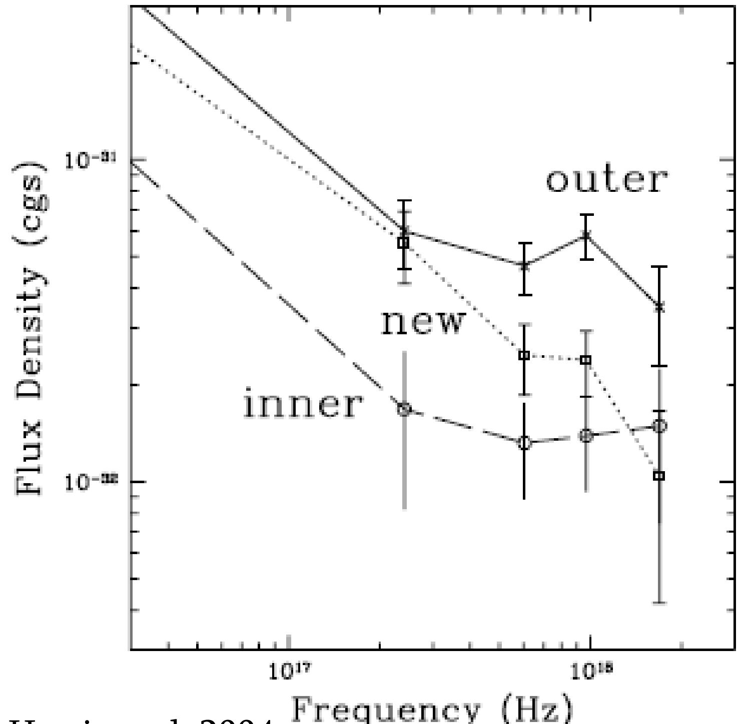

Harris et al. 2004

Both the proton synchrotron model and the electron self synchrotron model predict flux detectable by Fermi LAT

Gamma-ray emission from 3C 120

N. Sahakyan et al.: γ-rays from 3C 120

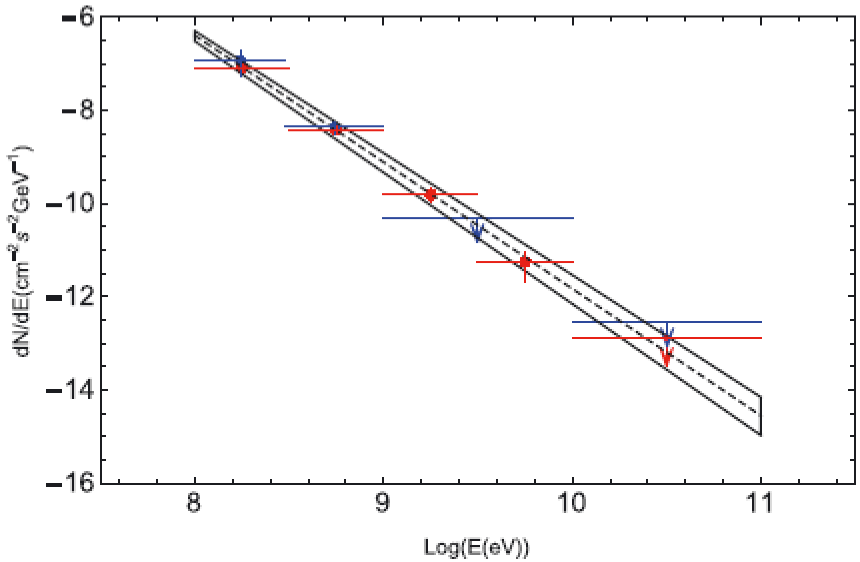

Fig. 1. Averaged differential spectrum of 3C 120 (above 100 MeV) red points as compared with that based on the initial 15 month data set (Abdo et al. 2010c). The dashed black line shows the power law function determined from the *gtlike*.

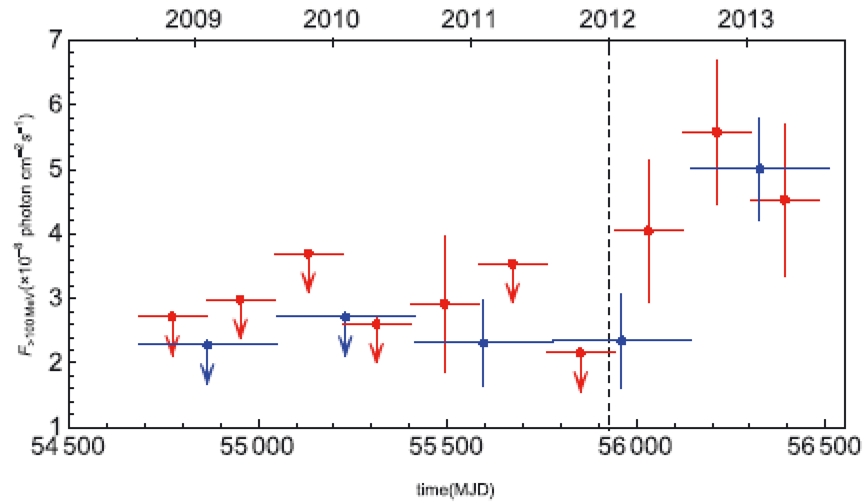

Fig. 2. Gamma-ray light curve from August 4th 2008 to December 4th 2013. The bin size corresponds to 180- (red) and 365-days (blue). The galactic and extragalactic background emission is fixed to the best-fit parameters obtained for the overall time fit.

Based on 5 years of data

New data analysis- flare

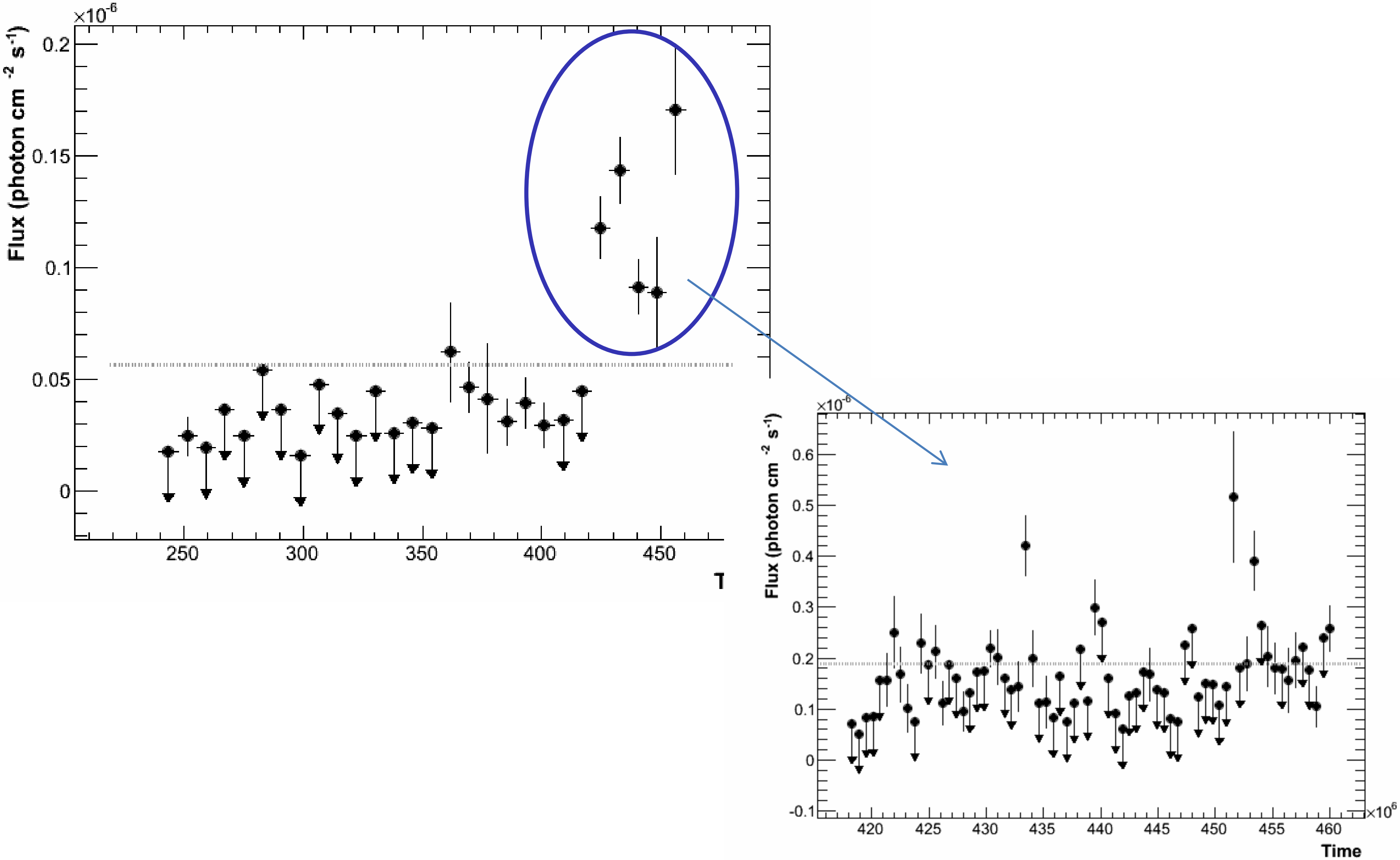

Spectrum: flare vs averaged

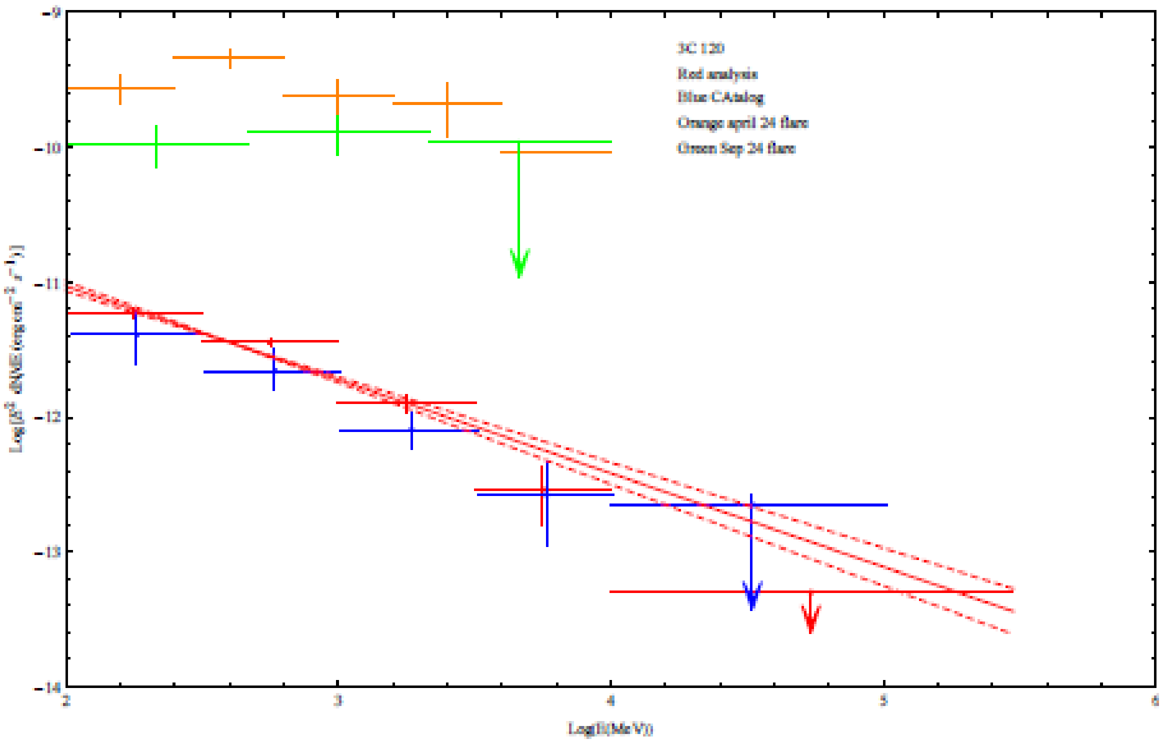

7-years averaged spectrum

$$\frac{dN}{dE} = (1.18 \pm 0.14) \times 10^{-12} \left(\frac{E}{1000} \right)^{-2.7 \pm 0.05} cm^{-2} s^{-1} MeV^{-1}$$

Flare-1

$$\left(\frac{dN}{dE} \right)_{APR.24} = (1.42 \pm 0.19) \times 10^{-10} \left(\frac{E}{1000} \right)^{-2.17 \pm 0.13} cm^{-2} s^{-1} MeV^{-1}$$

Flare-2

$$\left(\frac{dN}{dE} \right)_{SEP.24} = (5.31 \pm 1.21) \times 10^{-11} \left(\frac{E}{1000} \right)^{-2.26 \pm 0.22} cm^{-2} s^{-1} MeV^{-1}$$

Origin of gamma-rays

Synchrotron/Synchrotron self-Compton radiation)

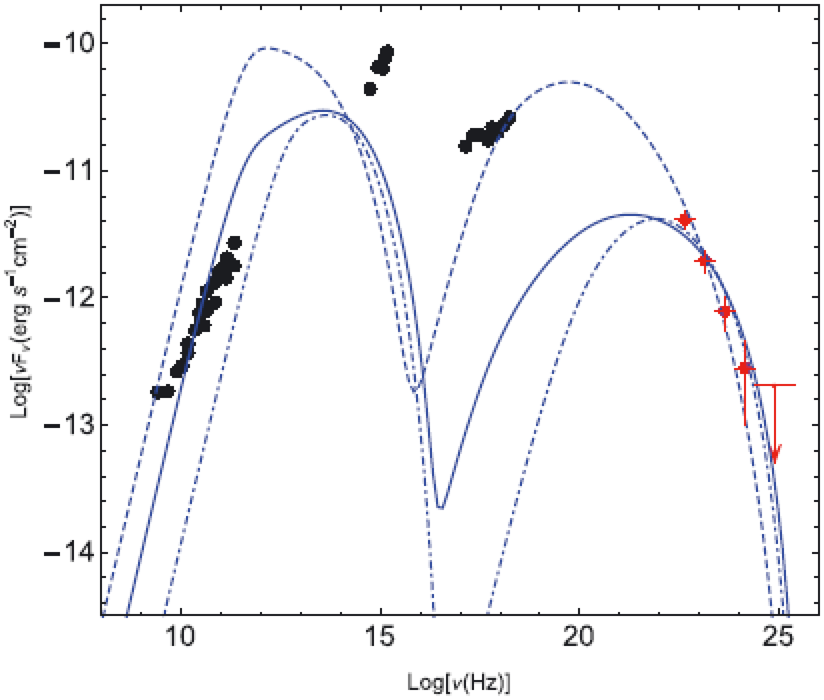

Monthly variability- emission region size

$$R_b \approx 10^{18}\, cm$$

Doppler boosting

$$\delta = 4$$

	B(mG)	α	$\gamma_{\min}$	γ_c	U_e/U_B
Solid line	30	2.4	700	1.7×10^4	1.9
Dashed line	25	2.8	800	9.8×10^3	16
Dot dashed line	25	2.0	2500	1.2×10^4	1.3

The jet luminosity $L_{jet} \approx 6 \times 10^{44}\, erg\, s^{-1}$ which corresponds to 10 % Eddington accretion power

Another example….

	B(G)	α	γ_{min}	γ_c	U_e/U_b
Solid line	0.18	2	100	11500	1
Dashed line	0.14	2	200	4500	8

$R_b \approx 10^{17} cm$

$\delta = 4$

3C 111

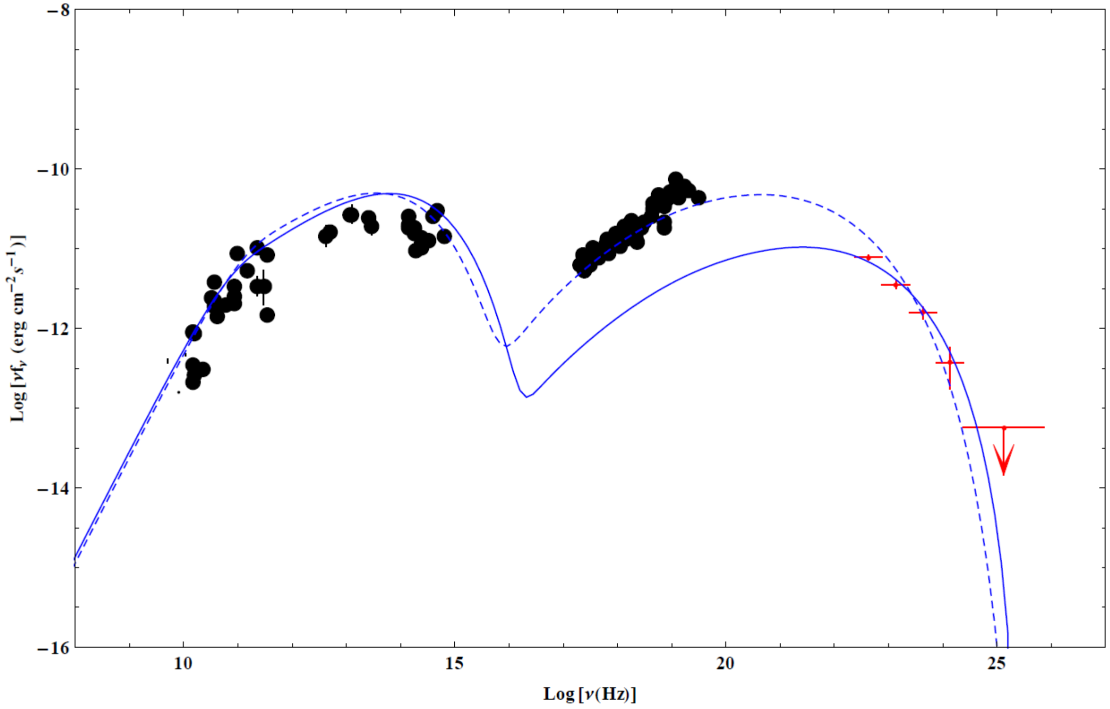

Conclusions

- The analysis of 7-year of Fermi LAT data from the observations of radio galaxies allows to investigate both the spectrum and variability.
- The spectra of several sources show deviation from a simple power-law modeling (NGC 6251, NGC 1275 etc)
- Strong variation of gamma-ray flux and photon index of NGC 1275 radio galaxy is found.
- The modeling of the emission from extended lobes of Cen A and Fornax A, indicates that the proton contribution can be significant.
- The analysis of simultaneous X-ray data will allow to reconstruct the nonthermal electron spectrum and investigate the particle acceleration/emission in the sub-parsec scale structures of radio galaxies.